学位請求論文

Study on Magneto-Optical Properties of Excitons in Quantum Nanostructures

量子ナノ構造における 励起子の磁気光学効果に関する研究

TANAKA, Takuji

田中　琢爾

A dissertation submitted to
the graduate school of University of Tokyo
in partial fulfillment of the requirements
for the degree of Doctor of Philosophy
in Electronic Engineering

December 20, 1995

Preface

This thesis describes an essential part of the research work carried out at the Institute of Industrial Science, and at the Research Center for Advanced Science & Technology, University of Tokyo, under the direction of Professor Yasuhiko ARAKAWA while the author was working as a graduate student of the Department of Electrical Engineering, University of Tokyo, from 1991 to 1995.

For future applications of tightly confined electrons and photons in low dimension to electronic and optoelectronic devices, clarification of physics in low dimensional freedom is significantly required. At the present time, great efforts in fabricating quantum nanostructures and multidimensional microcavity structures have realized the low dimensional states of electrons and photons, which have provided a potential of new excellent nanoscale devices.

In the present thesis, theoretical and experimental study on the magneto-optical properties of excitons in the quantum nanostructures is described. The author hopes this study contributes to accurate understanding of new phenomena in the electronic and optical confinement and its application to future novel devices.

TANAKA, Takuji

Roppongi, Tokyo

December 1995

Acknowledgements

The author would like to take this opportunity to thank my dissertation supervisor, Professor Yasuhiko ARAKAWA, Institute of Industrial Science (IIS), University of Tokyo, for his constant guidance and encouragement throughout my graduate studies at University of Tokyo. His valuable insights proved a great boon to my work, and being a member of his research group expanded my interests to many new areas of quantum electronics.

The author would like to thank his thesis committee Professor Y. FUJII, Professor T. KAMIYA, Professor H. SAKAKI, Professor U. NISHINAGA, and Professor K. HIRAKAWA, University of Tokyo for their time and input.

The author is grateful to Professor Y. FUJII, IIS, University of Tokyo, Professor H. SAKAKI, Research Center for Advanced Science & Technology (RCAST), University of Tokyo, and Dr. T. TAKAHASHI, RCAST, University of Tokyo for their constant guidance and encouragement.

The author is also grateful to thank Dr. J. N. SCHULMAN, Hughes Research Laboratories, Professor J. SINGH, University of Michigan, Professor G. W. E. BAUER, Delft University of Technology, for fruitful discussions and valuable collaboration.

The author would like to thank DR. Y. NAGAMUNE, RCAST, University of Tokyo (present: Electrotechnical Laboratory) for fruitful discussions and valuable suggestions.

The author wishes to thank Dr. I. OGURO, Institute of Solid State Physics, University of Tokyo for assistance and fruitful suggestions in measurements by superconducting magnet system.

The author would like to express my gratitude to Mr. M. NISHIOKA and Mr.

S. ISHIDA, whose technical assistance in the experimental aspects of this thesis was invaluable. The author is grateful to many other talented and helpful colleagues, Dr. S. TSUKAMOTO, Dr. Z. L. ZHANG, Dr. X. P. FENG, Mr. F. SOGAWA, Mr. T. YAMAUCHI, Mr. A. ISHIKAWA, Dr. sc M. Willatzen, Mr. T. ARAKAWA, Mr. T. KONO, Mr. H. NAKAYAMA, Mr. M. KITAMURA, Mr. H. WATABE, Mr. Y. KATOU, Mr. H. HAYASHI, Mr. R. SCHUR for their guidance, discussions and enjoyable collaboration.

The fellowship of the Japan Society for the Promotion of Science for Japanese Junior Scientists was generously supplied from 1993 April to 1996 March.

Finally, the author would like to express his sincere gratitude to his parents for their constant encouragement.

Contents

Chapter 1

Introduction

1.1 Background of this study

1.1.1 Magneto-optical effect in quantum nanostructures

The phenomena of high dimensionally confined particles are drastically different from those of free particles. Many studies on the physics of low dimensional carriers and photons in semiconductors have expected that those application to electronics and optoelectoronics will significantly improve performances of semiconductor devices [1–4]. The recent excellent fabrication techniques such as metalorganic chemical vapor deposition (MOCVD), molecular beam epitaxy (MBE), focused ion beam (FIB), electron beam lithography, etc. make it possible to fabricate nano-scale microstructure devices. For carriers, one dimensional (1D) confinement structures, quantum wells (QWs), can be grown with interface fluctuation less than one monolayer. Furthermore, two dimensional (2D) and three dimensional (3D) confinement structures such as quantum wires (QWRs) and quantum dots (QDs) have been realized [5,6]. For photons, microcavity structures with high Q lead to the 1D photon confinement. The even higher confinement structure [7], photonic crystal, will be realized in the near future.

In the field of even lower dimensional freedom of carriers, drastic change of carrier configuration is expected. The two dimensional QWs have been found to have superior characteristics of semiconductor lasers compared with conventional double heterostructure lasers [8]. The merits are expected to become more remarkable in QWRs and QDs [2,3]. Moreover, electrons in QWRs are predicted to have drastically enhanced mobility at low temperature compared to high electron mobility transistors (HEMTs) [4].

In order to clarify the physics of the low dimensional carriers, characterization of the quantum nanostructures comes to be more important since size fluctuation of the samples often conceals intrinsic low dimensional effects. Recently, the observation techniques with nano and sub-nano scale resolution such as scanning electron microscope (SEM), transmission electron microscope (TEM), atomic force microscope (AFM), scanning tunneling microscope (STM), etc. have allowed us to investigate atom-scale configuration of the structures. Furthermore, many optical measurements such as photoluminescence excitation (PLE), cathode luminescence (CL), micro-PL, magnetophotoluminescence (magneto-PL), photon STM etc. have confirmed carrier confinement effects in QWRs and QDs.

For characterization of carrier confinement in low dimensional structures, optical measurements under external magnetic fields [9–17] are useful because the carrier confinement can be directly controlled by the magnetic field. The effect of experimentally possible magnetic field (the order from one tesla to ten tesla) is enough sensitive to the nanostructures, because the magnetic field cause carrier confinement due to cyclotron motion equivalent to the quantized energy due to the confinement potential. In contrast to applied external electric field or external pressure, se-

lectability of the direction of the magnetic field allows us any direction of lateral confinement by cyclotron motion, which makes it possible to estimate the confinement effect along any directions.

In addition, magnetic field effect in quantum nanostructures is important to investigate the physics of the even lower dimensional carriers substituting for QWRs and QDs. A magnetic field applied normal to a QW cause carrier localization equivalent to a QD without imperfection of lateral confinement.

For the purpose mentioned above, magneto-optical properties of quantum nanostructures have been widely investigated. The magneto-photoluminescence (magneto-PL) measurements for QWRs [9–12] and QDs [13–17] have been reported, showing those carrier confinement effects, and used for estimation effective mass in the QWRs. Using this 'pseudo-QD', zero dimensional physics has been investigated for QD lasers [1] and transport in coupled QDs [18].

However, most of those works have obtained the magneto-optical properties on the basis of simple models neglecting some effects such as Coulomb interactions of electron–hole pairs, complex confinement potentials. The theoretical analyses of magneto-PL energy in quantum nanostructures have been obtained only for non–interacting particles in parabolic potentials [19–22]. Though inter-particle interaction in an anisotropic QD are analyzed for electron–electron correlation [23] and for electron–phonon interaction [24], the electron–hole interaction are included in theories for the special case of a QD with an isotropic parabolic confinement [16,25–29].

1.1.2 Control of exciton properties in quantum nanostructures by electromagnetic field

Photons confined in low dimensional optical cavities are expected to enable us to control of spontaneous emissions in the quantum nanostructures [30,31]. A quantum mechanical theory called cavity quantum electrodynamics (cavity QED) has deduced that spontaneous emission is controllable by modifying the mode distribution within a cavity [32]. In the field of atom and cavity system, many studies have found the controlled spontaneous emission by the cavity effect. In semiconductors, it is expected that inhibited and exhibited spontaneous emission due to strong electromagnetic field in optical microcavity makes possible control of exciton properties such as radiation lifetime. This phenomenon is predicted to improve performance of optical devices such as low threshold current of semiconductor lasers [33]. In order to clarify such cavity QED effects, proper understanding of photon–exciton interaction is important.

Thus, semiconductor microcavities with dimensions of one optical wavelength have attracted much attention to demonstrate the controlled spontaneous emission from QWs. The recent high technology to grow ultra thin semiconductor films have realized an optical microcavity of high Q in a semiconductor crystal using mirrors of high reflectivity such as distributed Bragg reflector (DBR). Moreover, the technology allowed us to get monolithic structures of a desired scheme with the optical microcavity and quantum nanostructures, which tightly confine photons and carriers, respectively, in a low dimension [34]. Recently, in QWs embedded in a microcavity (QWMC) structure, enhanced and inhibited spontaneous emission by strong coupling of photons and excitons have been observed [35–37]. Optical mea-

surements of QWRs [38] and QDs [39,40] embedded in a microcavity have been also reported. In the future, a composite structure with optical and carrier confinements in even lower dimensions may produce even stronger interaction between photons and excitons.

In QWMC structure, clear splitting of a resonant mode of exciton and photon has been found [41]. This is interpreted as the normal mode splitting of exciton polaritons due to a strong photon-exciton interaction, and is also as the vacuum-field Rabi splitting. Moreover, the coherent exciton-polariton emission with oscillation from resonantly excited excitons in a microcavity has been demonstrated [42,43], which is equivalent to the vacuum-field Rabi oscillation. These effects have been intensively investigated from the many aspects such as dependence on temperature [44–46], on electric field [44], on magnetic field [47], on excitation power [43,48], on number of QWs [49,50], on angle of emission [51] etc. and also controlled spontaneous emission [52] to much understand the properties of the photon–exciton interaction. These properties have been obtained by a quantum mechanical theory with Green function [53], and also with a model of a photon-exciton-coupled state, called 'dressed exciton', which has reversible spontaneous emission [54–56].

1.2 Objective and scope of this study

To characterize complex quantum nanostructures fabricated practically, it is important to estimate confinement effect along the interest direction by comparing properties more or less confined carriers to the expected. For instance, even using the most fine fabrication technique in these days, practical QWRs are hardly free from any defects or interface roughness, which force carriers to localize like a QD

or an intermediate state between a QWR and a QD. Fabricated QWRs and QDs may not be enough to laterally and vertically confine carriers. The possibility of those imperfection requires us to verify localization and confinement effects along the 'free' direction and the 'confined' direction. However, few detailed discussion [57] is achieved for properties of intermediate states between a QWR and a QD, or between a QW and a QD. To compare exciton properties among QWs, QWRs, QDs, and those intermediate structures and to investigate those dimensionality, theoretical analyses by an unified model for these structures should be important.

For investigation of low dimensional physics, magneto-optical properties of fabricated quantum nanostructures have been widely measured. However, most of those works have obtained the magneto-optical properties on the basis of simple models neglecting some effects such as Coulomb interactions between electron–hole pairs, complex confinement potentials.

Even though a magnetic field normal to any QWR with a simple structure, a external magnetic field applied to quantum nanostructures yields a condition with a complex anisotropic confinement. In addition, the fabricated quantum nanostructures have complex nanostructures. Moreover, quantum confinement, magnetic field, and electron–hole interactions are all expected to affect the optical properties of quantum nanostructures significantly with a same order of energies. Therefore, it is important to describe accurate carrier configuration of quantum nanostructures including all of the mechanisms, quantum confinement, magnetic field, and electron–hole interactions, in the analysis of magneto-optics.

As mentioned above, the magnetoexciton properties in low dimensional structures is important to investigate physics of even lower dimensions and to examine

fabricated quantum nanostructures. From this view point, cavity photon effect on the magnetoexciton is also important to clarify interaction between magnetoexciton and photon such as estimation of exciton oscillator strength of magnetoexcitons in the optical cavity. The low dimensional freedom of carriers and the optical field, and those combination may lead to yet new physical phenomena.

The purpose of the present study is to show the importance of accurate understanding of the magnetoexciton properties in quantum nanostructures and microcavities to clarify the physics of low dimensional carriers and photons. This study presents a unified theory for all confinement dimensions, i.e. QDs, QWRs, QWs, and those intermediate structures in order to describe dimensionality of quantum confinement effect. Moreover, properties of magnetoexcitons in quantum nanostructures are also analyzed including all of the expected mechanisms: anisotropic quantum confinement, magnetic field, and, electron–hole interactions, comparing to experimental measurements of magneto-optics for quantum nanostructures. In addition, a 3D Schrödinger equation including external magnetic field is solved for the structural dependence on the varied direction of applied magnetic fields. Furthermore, magneto-optical effect is examined for the interaction between magnetoexcitons and microcavity photons. The measurement of the dependence of the magnetoexciton polariton mode splitting on the magnetic field is presented with a theoretical analysis. Moreover, the cavity photon effect on the magnetoexciton is discussed.

1.3 Synopses of chapters

In the present study, the magnetoexciton properties in quantum nanostructures and microcavities are investigated to clarify the phenomena of low dimensional carriers

and photons. This thesis is organized as follows.

Chapter 2 first introduces a theory assuming anisotropic 3D parabolic potential. Analytical solution for a single particle in the magnetic field and numerical calculation procedure by a variational method for the magnetoexciton effect in the confinement structure are described. Next, we discuss the exciton properties calculated by this model for QWs, QWRs, QDs, and intermediate dimensional quantum nanostructures with and without magnetic field.

Chapter 3 theoretically discusses the dependence of magnetoexciton properties on the confinement structures of QWRs by the variational method and by a 3D Schrödinger equation. Furthermore, the results of numerical calculation for the magneto-PL of QWRs are compared to the experimental results of previous works. The mutual relation between quantum confinement, magnetic field, and the exciton effect are minutely discussed.

Chapter 4 reports the measurement and the theoretical analysis of the exciton-polariton mode splitting under a high magnetic field up to 14.5 T with different number of QWs embedded in microcavity. The dependence of the strength of interaction between magnetoexciton and photon on the magnetic field is discussed with a theoretical analysis.

Chapter 5 expresses the conclusion of this thesis.

Chapter 2

Theory on Magnetoexcitons in Quantum Nanostructures

abstract

Exciton properties quantum dots (QDs) and quantum wires (QWRs) with an anisotropic three-/two- dimensional parabolic potential in a magnetic field are studied. The analytical solution is obtained for the single–particle states in the anisotropic confinement under the magnetic field. Energy states, wavefunction, and exciton oscillator strength are analyzed numerically including Coulomb interaction between an electron–hole pair for the QDs, QWRs, quantum wells, and intermediate dimensional nanostructures.

2.1 Introduction

Recently, nano-scale fabrication techniques have realize several types of quantum wires (QWRs) and quantum dots (QDs) of high quality, which have very complex structures. In order to clarify the physics of the low dimensional carriers, characterization of the quantum nanostructures comes to be more important. To this purpose, it is important to estimate confinement effect along the interest direction by comparing properties more or less confined carriers to the expected. The possibility of structural imperfection requires us to verify localization and confinement effect along the 'free' direction and the 'confined' direction. In addition, the complex structures of the fabricated QWRs and QDs are expected to cause complex quantum confinement effects which may not approximate by a single dimensionality. However, few detailed discussion [57] is achieved for properties of intermediate states between a QWR and a QD, or between a quantum well (QW) and a QD. To compare exciton properties among QWs, QWRs, QDs, and those intermediate structures and to investigate those dimensionality, theoretical analyses by an unified model for these structures should be important.

In order to characterize carrier confinement in low dimensional structures, optical measurements under external magnetic fields are useful because we can directly control the confinement of the carriers by the magnetic field. In addition, magnetic field effect in quantum nanostructures is important to investigate the physics of the even lower dimensional carriers substituting for QWRs and QDs with some imperfection. In fact, many magneto-optical measurements of QWRs and QDs have reported, showing their low dimensional confinement effect. To clarify the magneto-

optical effects in the QWRs and QDs, it is important to investigate accurate carrier configuration of quantum nanostructures with an realistic confinement potential in a magnetic field.

However, most previous analyses of the measured magneto-PL of quantum nanostructures, especially those of QWRs, have been compared a simple model which neglected the exciton binding energy [9]. The analytical solution of magneto-PL energy in quantum nanostructures have been obtained only for non–interacting particles in parabolic potentials [19–22]. Recently, exciton properties of QDs in a magnetic field were analyzed for the special case of an isotropic parabolic confinement [16, 25–29]. In addition, the inter-particle interaction for an anisotropic QD are discussed for electron–electron correlation [23] and for electron–phonon interaction [24].

Even though a magnetic field normal to any QWR with a simple structure, a external magnetic field applied to quantum nanostructures yields a condition with a complex anisotropic confinement. In addition, the fabricated quantum nanostructures have complex structural configuration. Moreover, complex boundary condition of quantum confinement, magnetic field, and electron–hole interactions are all expected to affect the optical properties of QWRs significantly with a same order of energies. Therefore it is important to include all of these mechanisms in the analysis of the optical properties.

This chapter first derive the analytical solution of the energy levels of a single carrier gas confined by an anisotropic three dimensional (3D) parabolic potential in the presence of a magnetic field without considering Coulomb effect. Then, it is introduced that a numerical calculation procedure by a variational method for the magnetoexciton effect in the anisotropic two dimensional (2D) and 3D confine-

ment, i.e. the effect of Coulomb interaction in the presence of a QWR and a QD potential under an external magnetic field. Next, from the view point of the confinement by intermediate quantum nanostructures, we discuss the results calculated by this model. To clarify exciton states by this model, exciton binding energy and wavefunctions without external magnetic field is shown. Finally, comparing these structures, the dimensionality for the dependence of exciton oscillator strengths on the magnetic field are discussed. We minutely discuss the mutual relation between quantum confinement, magnetic field, and the exciton effect in the next chapter, referring to structure dependence of the magneto-PL in QWRs. To the best of our knowledge, this theoretical analysis of the magneto-PL in quantum nanostructures includes one dimensional (1D) and anisotropic zero dimensional (0D) exciton effect for the first time.

2.2 Theory

2.2.1 Analytical Solution for a single carrier

The Hamiltonian of an electron–hole pair with Coulomb interaction is

$$\mathscr{H}_{e,h,\mathrm{C}} = \mathscr{H}_e + \mathscr{H}_h + \mathscr{H}_{\mathrm{C}}, \tag{2.1}$$

where $\mathscr{H}_{\mathrm{C}} = -e/4\pi\varepsilon r$, $r = \sqrt{(x_e - x_h)^2 + (y_e - y_h)^2 + (z_e - z_h)^2}$, ε is the permittivity, and $\mathscr{H}_j$ is the Hamiltonian of a single–particle (an electron or a hole denoted by $j = e, h$, respectively). Quantum structures (QDs, QWRs, and QWs) are assumed to be defined by a parabolic confinement potential. The single–particle Hamiltonian $\mathscr{H}_j$ of the structure in a magnetic field is then

$$\mathscr{H}_j = \frac{(\mathbf{P}_j + q\mathbf{A}_j)^2}{2m_j{}^*} + \sum_{\zeta=x,y,z} \frac{1}{2} m_j{}^* \omega_{\zeta,j}{}^2 \zeta_j{}^2, \tag{2.2}$$

where $\omega_{\zeta,j}$ ($\zeta = x, y, z$) is the oscillator frequency of the parabolic potential along the ζ_j direction, $m_j{}^*$ is the isotropic effective mass and q is the electron charge. If two (one, none) of $\omega_{x,j}$, $\omega_{y,j}$ and $\omega_{z,j}$ are (is) equal to zero, the structure is a QW (QWR, QD), respectively.

First, we describe the analytical solution for the Hamiltonian $\mathscr{H} = \mathscr{H}_j$ (the subscript j is omitted below) of a single-particle in a magnetic field B along the z axis without Coulomb interaction. A gauge with the vector potential $\mathbf{A} = B(-w^2 y, v^2 x, 0)$ is used, where $v = \sqrt{\omega_x/(\omega_x + \omega_y)}$ and $w = \sqrt{\omega_y/(\omega_x + \omega_y)}$. The eigenfunction of the Hamiltonian $\mathscr{H}$ can be separated into functions of (x, y) and z. The eigenenergy of the Hamiltonian is expressed as the sum of eigenenergies along the (x, y)-plain (perpendicular to the magnetic field $\mathbf{B}$) $E^{(x,y)}$ and along the z axis (parallel to the magnetic field $\mathbf{B}$) $E^{(z)}$. The eigenenergy along the z axis parallel to the magnetic field is

$$E^{(z)} = \begin{cases} (l + \frac{1}{2})\hbar\omega_z & (\omega_z \neq 0) \\ \dfrac{{p_z}^2}{2m^*} & (\omega_z = 0) \end{cases}, \tag{2.3}$$

where p_z is the momentum of a plane wave along the z axis, and l is an integer.

The problem of a carrier in the (x, y)-plane perpendicular to the magnetic field along the z axis is solved as follows. The single-particle Hamiltonian along (x, y)-plane taking into account of harmonic confinement and magnetic field is

$$\mathscr{H}^{(x,y)} = -\frac{(\mathbf{P} + q\mathbf{A})^2}{2m^*} + \frac{1}{2}m^*\omega_x x^2 + \frac{1}{2}m^*\omega_y y^2. \tag{2.4}$$

When $\omega_\xi \neq 0$ and $\omega_\eta = 0$ ($\xi,\ \eta = x,\ y$), the analytical solution of the Schrödinger equation is obtained [19] as follows. The wavefunction is given by

$$\Phi = H_n(\zeta)\exp(-\zeta^2/2 + ip_\xi\xi/\hbar), \tag{2.5}$$

using the Hermite polynomials

$$H_n(t) = \sum_{r=0}^{[n/2]} (-1)^r (2r-1)!! \begin{pmatrix} n \\ 2r \end{pmatrix} 2^r t^{n-2r}, \tag{2.6}$$

where

$$\zeta = \begin{cases} \sqrt{\frac{m^*\omega_0}{\hbar}} y + \frac{p_x \omega_c}{\sqrt{m^* \hbar \omega_0^3}}, & (\omega_x = 0) \\ \sqrt{\frac{m^*\omega_0}{\hbar}} x - \frac{p_y \omega_c}{\sqrt{m^* \hbar \omega_0^3}}, & (\omega_y = 0), \end{cases} \tag{2.7}$$

$$\omega_0 = \sqrt{{\omega_c}^2 + (\omega_x + \omega_y)^2}, \tag{2.8}$$

$$\omega_c = \frac{qB}{m^*} \tag{2.9}$$

is cyclotron frequency, and p_ξ is momentum of plane wave along ξ axis. The wavefunction has the eigenenergy

$$E_{n,p_\xi} = (n + \frac{1}{2})\hbar\omega_0 + \frac{{p_\xi}^2}{2m^*} \frac{{\omega_\xi}^2}{{\omega_0}^2}, \tag{2.10}$$

where $n = 0, 1, 2, \ldots$.

When $\omega_x \omega_y \neq 0$, we substitute the variables as follows

$$X = vx\sqrt{m^*\omega_0/\hbar}, \tag{2.11}$$

$$Y = wy\sqrt{m^*\omega_0/\hbar}. \tag{2.12}$$

Then, the Hamiltonian is described by

$$\begin{aligned} \mathscr{H} &= E_0 \left\{ v^2 \left(-\frac{\partial^2}{\partial X^2} + X^2 \right) + w^2 \left(-\frac{\partial^2}{\partial Y^2} + Y^2 \right) \right\} \\ &\quad -2iuvE_c \left(X\frac{\partial}{\partial Y} - Y\frac{\partial}{\partial X} \right), \end{aligned} \tag{2.13}$$

where

$$E_0 = \hbar\omega_0/2, \tag{2.14}$$

$$E_c = \hbar\omega_c/2. \tag{2.15}$$

Moreover, we can make the ansatz

$$\Psi = \Phi \exp(-X^2/2 - Y^2/2), \tag{2.16}$$

The Schrödinger equation $\mathscr{H}\Psi(x,y) = E\Psi(x,y)$ is then transformed into $\mathscr{H}_1\Phi = (E - E_0)\Phi$, where

$$\begin{aligned}\mathscr{H}_1 &= E_0 v^2\left(-\frac{\partial^2}{\partial X^2} + 2X\frac{\partial}{\partial X}\right) + E_0 w^2\left(-\frac{\partial^2}{\partial Y^2} + 2Y\frac{\partial}{\partial Y}\right) \\ &\quad -2ivwE_c\left(X\frac{\partial}{\partial Y} - Y\frac{\partial}{\partial X}\right).\end{aligned} \tag{2.17}$$

Furthermore, the wavefunction can be expanded by basis functions

$$u_{k,m} = \frac{H_m(X)H_{k-m}(Y)}{\sqrt{m!(k-m)!}}, \tag{2.18}$$

$(k = 0, 1, 2, \ldots;\ m = 0, 1, 2, \ldots, k)$. Then Hamiltonian $\mathscr{H}_1$ is determined by the matrix $(\langle u_{k,j}|\,\mathscr{H}_1\,|u_{k,j'}\rangle)$ with dimension $(k+1)\times(k+1)$ as follows

$$\mathscr{H}_1 = E_0 I_k - (v^2 - w^2)E_0 A_k - vwE_c B_k, \tag{2.19}$$

where

$$I_k = \begin{bmatrix} k & & & & & \\ & k & & & & 0 \\ & & k & & & \\ & & & \ddots & & \\ & & & & k & \\ 0 & & & & & k \end{bmatrix} \tag{2.20}$$

$$A_k = \begin{bmatrix} k & & & & & \\ & k-2 & & & & 0 \\ & & k-4 & & & \\ & & & \ddots & & \\ & & & & -k+2 & \\ 0 & & & & & -k \end{bmatrix} \tag{2.21}$$

$$B_k = \begin{bmatrix} 0 & -i\sqrt{k} & & & & & \\ i\sqrt{k} & 0 & -i\sqrt{k-1}\sqrt{2} & & & & \\ & i\sqrt{k-1}\sqrt{2} & 0 & -i\sqrt{k-2}\sqrt{3} & & & \\ & & i\sqrt{k-2}\sqrt{3} & 0 & \ddots & & \\ & & & \ddots & \ddots & & \\ & & & & i\sqrt{2}\sqrt{k-1} & 0 & -i\sqrt{k} \\ 0 & & & & & i\sqrt{k} & 0 \end{bmatrix} \tag{2.22}$$

The eigenenergy $E_{k,m}^{(x,y)}$ of the Schrödinger equation can be found by diagonalizing this matrix:

$$E_{k,m} = (1+k)E_0 + (k-2m)E_1, \tag{2.23}$$

where $E_0 = \frac{1}{2}\hbar\sqrt{\omega_c + (\omega_x+\omega_y)^2}$, $E_1 = \frac{1}{2}\hbar\sqrt{\omega_c + (\omega_x-\omega_y)^2}$. This eigenenergy can be written by quantum numbers $l = 0, \pm1, \pm2, \ldots$; $n = 0, 1, 2, \ldots$, as

$$E_{n,l} = (2n+1+|l|)E_0 + lE_1. \tag{2.24}$$

This eigenenergy is equal to the value obtained in a somewhat different context [20,23,24]. In the isotropic case of $\omega_x = \omega_y$, the eigenvalue is equal to the value given by Fock [21,22]. In the present study, we focus on the ground state with the energy $E = E_0 + \frac{1}{2}\hbar\omega_z$ and the eigenfunction along the (x,y)-plane $\Psi = \exp(-\frac{1}{2}X^2 - \frac{1}{2}Y^2)$.

Figure 2.1 shows configuration of energy levels, where $\Delta E_- = E_0 - E_1$, $\Delta E_+ = E_0 + E_1$, $\Delta E_0 = 2E_0$. Figure 2.2 shows the contours of energy components E_0 and E_1 of the eigenenergy of Eq. (2.25) and energy separations ΔE_- and ΔE_+ which depend on the ratios of oscillator frequency of the harmonic potentials (ω_x, ω_y) to the cyclotron frequency (ω_C). The first excited level is

$$E_{n=0,l=\overline{1}} = E_0 + \Delta E_-. \tag{2.25}$$

If $\omega_x + \omega_y$ and ω_c are fixed, i.e. if confinement energy and magnetic field are fixed, the

first excited energy is smaller for the structure with more anisotropic confinement i.e. ω_x or ω_y is smaller. At the limit of the anisotropy, ΔE_- approaches zero. In addition, as magnetic field B is more enhanced compared to 2D confinement ($\omega_c \gg \omega_x, \omega_y$), the energy levels are closer to Landau levels.

2.2.2 Variational method for magnetoexcitons

In the following, we discuss our numerical method for the magneto-exciton effect on an electron–hole pair in the QWR. The variational method is used for the Hamiltonian $\mathscr{H}_{e,h,\mathrm{C}}$ determined by Eq. (2.1). We assume a variational function of the form

$$\Psi_{e,h,\mathrm{C}} = \phi_1 \phi_2, \tag{2.26}$$

where

$$\phi_1 = \exp\left(-\sum_{j=e,h}\left(\alpha_{x,j}{x_j}^2 + \alpha_{y,j}{y_j}^2 + \alpha_{z,j}{z_j}^2\right)\right), \tag{2.27}$$

$$\phi_2 = \exp(-\beta r), \tag{2.28}$$

and $\alpha_{\zeta,j}$, β are variational parameters. ϕ_1 is the Gaussian function which gives the correct eigenfunction for the Hamiltonian $\mathscr{H}_e + \mathscr{H}_h$, describing the effect of the 2D parabolic confinement and of the magnetic field. ϕ_2 is the hydrogenic function which gives the correct eigenfunction for the Hamiltonian $\mathscr{H}_{\mathrm{C}}$, describing the effect of the Coulomb force. The energy is computed as

$$E_{e,h,\mathrm{C}} = \min \frac{\langle \Psi_{e,h,\mathrm{C}} | \mathscr{H}_{e,h,\mathrm{C}} | \Psi_{e,h,\mathrm{C}} \rangle}{\langle \Psi_{e,h,\mathrm{C}} | \Psi_{e,h,\mathrm{C}} \rangle}. \tag{2.29}$$

The exciton binding energy of the system is defined as $E_{\mathrm{C}} = E_e + E_h - E_{e,h,\mathrm{C}}$. We parametrize the parabolic confinement potentials in terms of equivalent widths L_ζ, which are chosen such that the ground state single particle energies $\frac{1}{2}\hbar\omega_{\zeta,j}$

agree with that of an infinite barriers square well $\hbar^2\pi^2/2m_j{}^*L_\zeta{}^2$. The term of $\langle\Psi_{e,h,\mathrm{C}}|\,\mathscr{H}_{e,h,\mathrm{C}}\,|\Psi_{e,h,\mathrm{C}}\rangle$ and $\langle\Psi_{e,h,\mathrm{C}}|\Psi_{e,h,\mathrm{C}}\rangle$ in Eq. (2.29) includes the integral

$$I_n = \int_0^\infty r^n \exp(-Ar^2/2 - Br)dr, \tag{2.30}$$

which requires numerical calculation. The method of this calculation is described in Appendix A.

2.3 Excitons in quantum wires and quantum dots

2.3.1 Exciton binding energy of quantum nanostructures

Figure 2.3 shows calculated exciton binding energies E_C of the following quantum structures: (a) a QW with $L_z = L_\mathrm{W}, L_x = L_y = \infty$, (b) a QWR with $L_x = L_y = L_\mathrm{W}, L_z = \infty$, and (c) a QD with $L_x = L_y = L_z = L_\mathrm{W}$, using the material parameters of bulk GaAs: $m_e{}^* = 0.067m_0$, $m_h{}^* = 0.45m_0$, and $\varepsilon = 12.8\varepsilon_0$. In quantum well, the static dielectric constant ϵ under a perturbing electric field is known to be reduced by quantum confinement effect and have an anisotropy along the direction of the electric field [58]. However, the reduction of ϵ is small in the parameter regime of our interest (larger than 30 Å). Therefore, we used an isotropic ε of bulk GaAs. At $L_\mathrm{W} = \infty$, the calculated exciton binding energy E_C of all three structures reaches the bulk exciton value of $m_r{}^*e^4/32\pi^2\varepsilon^2\hbar^2 \simeq 4.8$ meV where $m_r{}^* = m_e{}^*m_h{}^*/(m_e{}^* + m_h{}^*)$ is the reduced effective mass. In addition, at $L_\mathrm{W} = 0$, E_C of the QW reaches the analytical value $m_r{}^*e^4/8\pi^2\varepsilon^2\hbar^2 \simeq 19.4$ meV [59]. In this case, the exciton wavefunction is a delta function along the confined direction and a hydrogenic function along the QW plane [59], and is asymptotically given by our variational function $\Psi_{e,h,\mathrm{C}} = \phi_1\phi_2$ with the parameters $\alpha_{x,j}, \alpha_{y,j} \to \infty$, $(j = e, h)$.

Moreover, our calculated exciton binding energies for the QWR and the QD are consistent with the results by the previous works [25,60,61].

2.3.2 Exciton states in intermediate quantum nanostructures

In following, we discuss the exciton properties in intermediate dimensional quantum nanostructures from QD to QWR and from QWR to QW in our model. First, for a QD with variable confinement along one axis (z) and fixed confinement along other axes (x, y), we have calculated (a) exciton binding energy E_C and (b) root mean square of relative separation $\sqrt{\langle(\zeta_e - \zeta_h)^2\rangle}$ along the ζ ($\zeta = x, y, z$) axis. The results are shown in Fig. 2.4. In Fig. 2.4(b), it is seen that the relative separation is not much changed along x, y, but increases strongly with L_z until it reaches a constant corresponding to the exciton radius of the QWR.

For a QWR with variable confinement along one axis (y), fixed confinement along the other axis (x) and free along the other axis (z), the calculated results of (a) exciton binding energy E_C and (b) root mean square of relative separation $\sqrt{\langle(\zeta_e - \zeta_h)^2\rangle}$ along the ζ ($\zeta = x, y, z$) axis are shown in Fig. 2.5. In Fig. 2.5(b), it is seen that the relative separation is not much changed along the direction with fixed confinement x, but increases strongly with L_y until it reaches a constant corresponding to the exciton radius of the QW. The relative separation along the free axis z slightly depends on L_y, showing shrinkage of exciton wavefunction with decrease of L_y even along the free direction.

A different measure of the exciton states is provided by the normalized parameter

$$t_\zeta = \beta/\sqrt{2\alpha_\zeta}, (\zeta = x, y, z) \tag{2.31}$$

where $1/\alpha_\zeta = 1/\alpha_{\zeta,e} + 1/\alpha_{\zeta,h}$. t_ζ describes the character of the variational function along the ζ axis, which can be more Gaussian-like ($t_\zeta \to 0$) or more hydrogen-like ($t_\zeta \to \infty$). Figure 2.6 shows the dependence of the parameter t_ξ on the confinement length. for (a) a quantum dot which has various dimension along one axis (z) and fixed dimension along other axes ($L_x = L_y = 100$ Å), and for (b) a quantum wire which has various dimension along one axis (y) and fixed dimension along other axes ($x = 100$ Å, $z = \infty$). In Fig. 2.6(a), when $L_z \gg L_x, L_y$, the parameters are related as $t_z > t_x, t_y$. When $L_z \ll L_x, L_y$, as $t_z < t_x, t_y$. In Fig. 2.6(b), when $L_y \gg L_x$, the parameters are related as $t_y > t_x$. When $L_y \ll L_x$, as $t_y < t_x$. These results show that the wavefunction is more hydrogen-like along the direction which is less tightly confined by the parabolic potential. On the other hand, the wavefunction is more Gaussian-like along the direction which is more tightly confined.

2.4 Magnetoexciton oscillator strength in quantum nanostructures

In this section, we discuss exciton oscillator strength in QWs, QWRs, and QDs systematically using a unified formula for the multi-dimensional confinements. The enhancement strength of magneto-PL is compared to an experiment.

The exciton oscillator strength is proportional to the probability that the separation between the electron and the hole is equal to zero: $f_{\rm ex} \propto |\phi_{\rm ex}(\mathbf{r}_e - \mathbf{r}_h = 0)|^2$, and other parameters hardly affect on the oscillator strength [62].

Figure 2.7 shows the probability $|\phi_{\rm ex}(0)|^2$ for a QW, a QWR, and a QD with the dimension along confined axis (axes): $L_z = 80$ Å, $L_y/2 = L_z = 80$ Å, and $L_x/2 = L_y/2 = L_z = 80$ Å, respectively, as a function of magnetic fields applied

along the z axis. The parameters used are electron mass $m_e = 0.067m_0 \times 1.35$, hole mass $m_h = 0.48m_0$, and permittivity $\epsilon = 12.8\epsilon_0$. We considered the enhancement of the electron mass in the high dimensionally confined structures [63]. These parameters is as same as that used in Section 3.3, Chapter 3 for the magneto-PL of the QWRs with various lateral widths, where calculation accurately describe the energy shifts. Figure 2.7 shows the confinement in the lower dimension enhances exciton oscillator strength, while the shift of oscillator strength due to the magnetic field is suppressed. In high magnetic field range, the shift comes to be independent on the dimensionality because the exciton states reach Landau shift which is not affected by the confinement potential. The state transform from that mainly affected by quantum confinement to that of the Landau-like is found at $\omega_C = \omega_x + \omega_y$, as same as noninteracting single particle mentioned in Section 2.2. Therefore, the shift strongly depends on the mutual relation between the confinement by magnetic field and potential. These properties are equivalent to that of the quantized energy discussed in Chapter 3 in detail.

In addition, the experimental magneto-PL intensity [64] fits the calculation without any additional fitting parameters. Thus, the theory seems consistent with the experiment.

2.5 Conclusion

In this chapter, we first described the analytical solution of energy levels of a one dimensional (1D) carrier confined by an anisotropic 2D parabolic potential in the presence of a magnetic field. The exciton properties was calculated by the theory assuming anisotropic 3D parabolic potential and coulomb interaction within an

electron–hole pair. For QWs, QWRs, QDs, and intermediate dimensional quantum nanostructures with and without magnetic field, the exciton properties such as binding energy, wavefunction, and exciton oscillator strength are calculated.

The magnetic field effect on those exciton properties is found to strongly depend on the mutual relation between the confinement by magnetic field and potential. These results show magneto-optical measurement is important for the characterization of the quantum nanostructures.

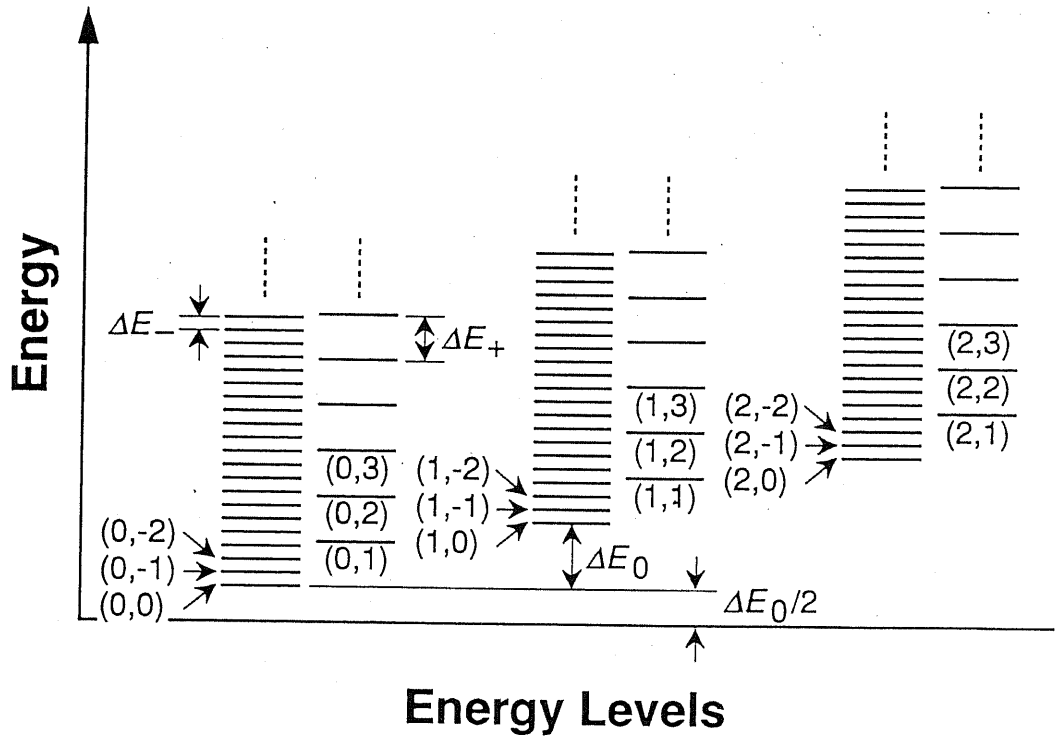

Figure 2.1: Distribution of energy levels. (n, l) denotes quantum numbers which indicates the eigenstate with the eigenenergy $E_{n,l}$ of Eq. (2.25).

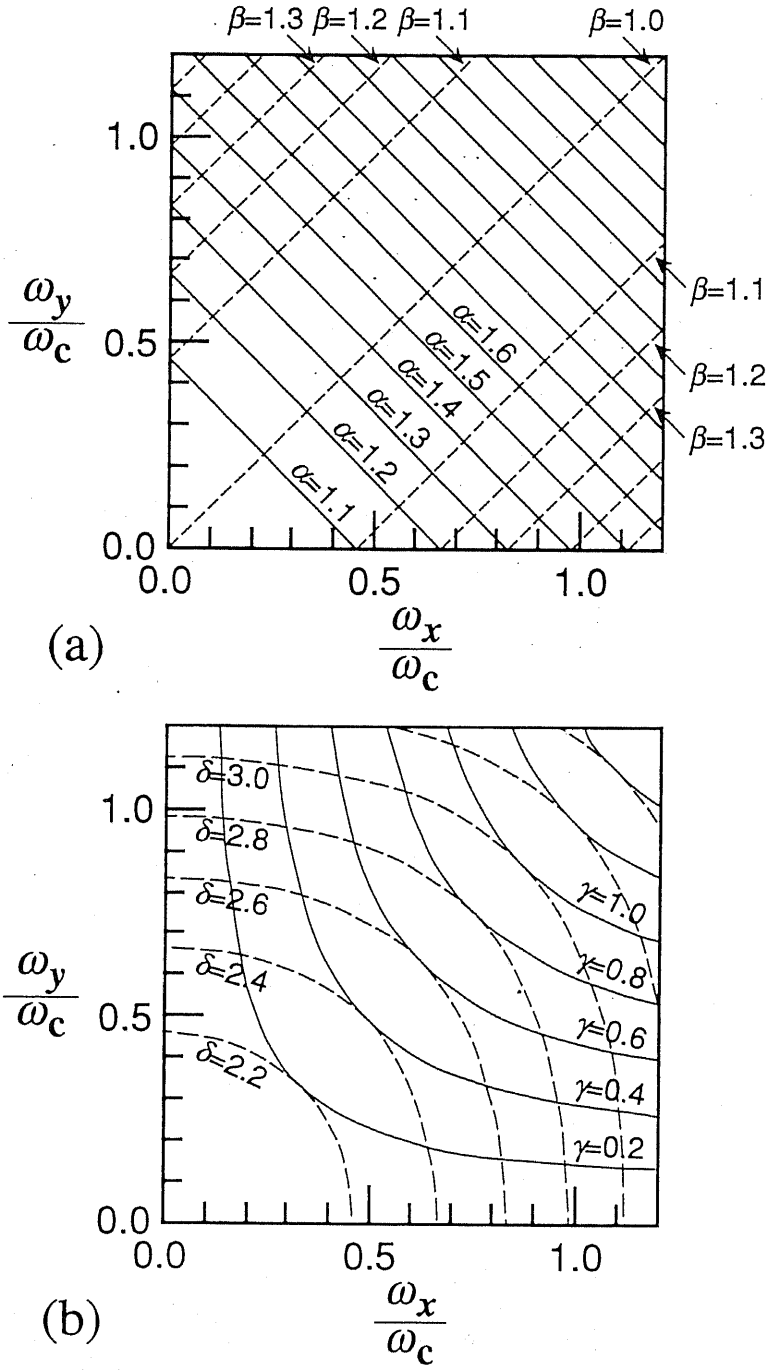

Figure 2.2: Contours of (a) energy components the eigenenergy of Eq. (2.25): E_0 (solid line), E_1 (dashed line), and (b) energy separations ΔE_- (solid line), ΔE_+ (dashed line), which depend on the oscillator frequency of the harmonic potentials (ω_x, ω_y) and the cyclotron frequency (ω_C). α, β, γ, and δ denotes normalized energy component and separation: $E_0/(\hbar\omega_C/2)$, $E_1/(\hbar\omega_C/2)$, $\Delta E_-/(\hbar\omega_C/2)$, and $\Delta E_+/(\hbar\omega_C/2)$, respectively.

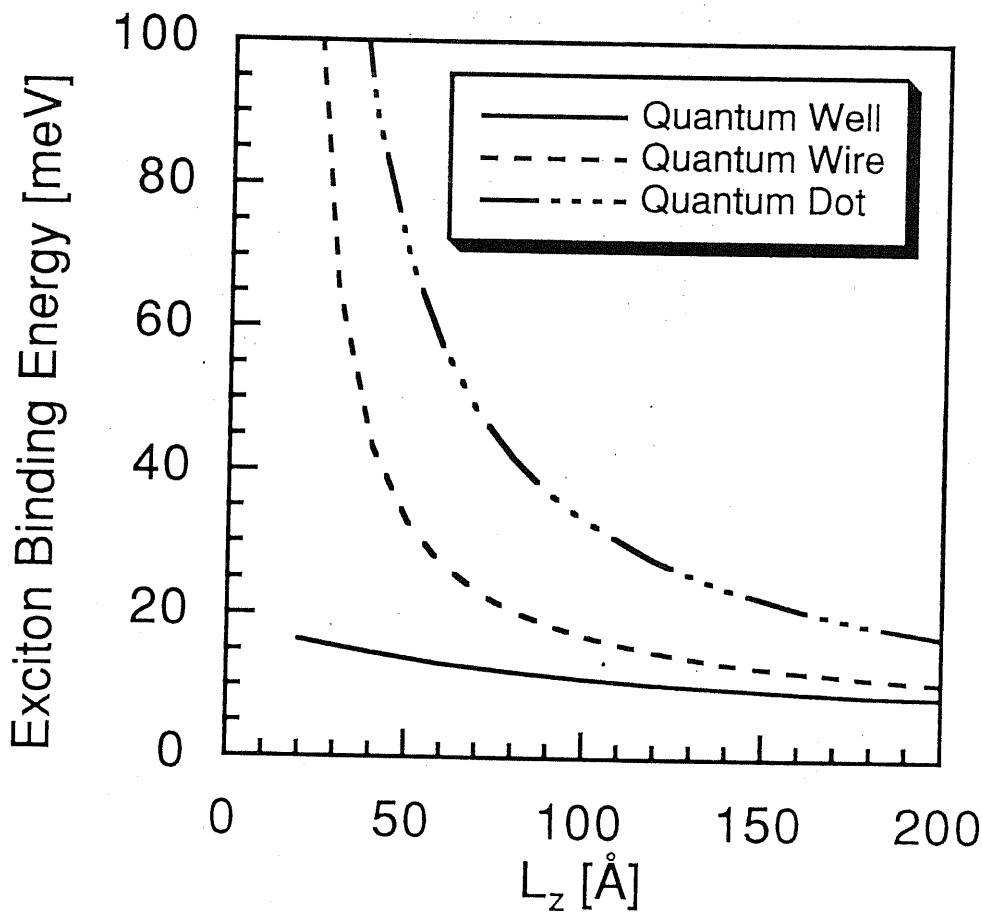

Figure 2.3: Exciton binding energies of quantum structures: (a) quantum well with $L_z = L_W, L_x = L_y = \infty$, (b) quantum wire with $L_x = L_y = L_W, L_z = \infty$, (c) quantum dot with $L_x = L_y = L_z = L_W$.

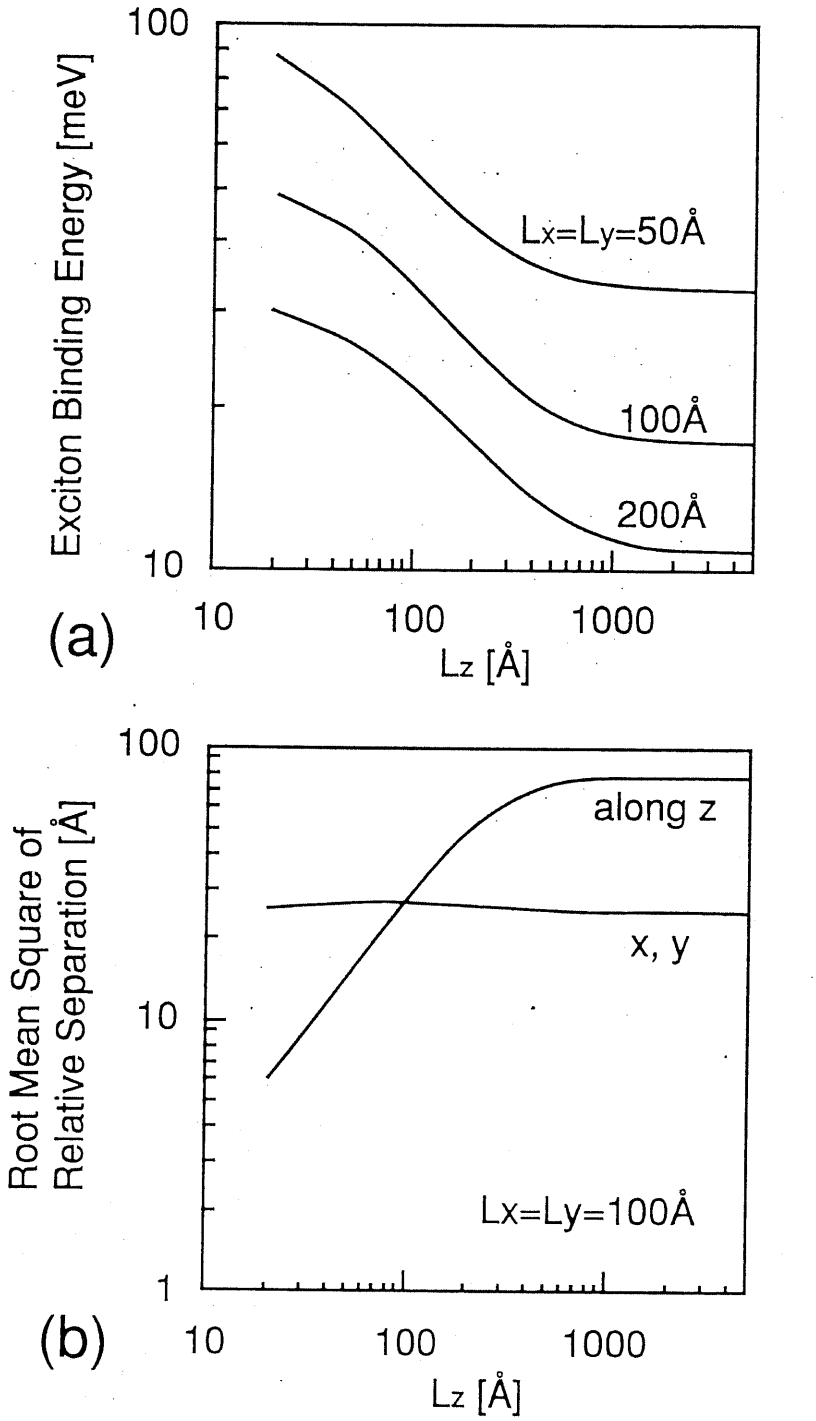

Figure 2.4: a) Exciton binding energy E_C and (b) root mean square of electron-hole separation in the ground state $\sqrt{\langle(\zeta_e - \zeta_h)^2\rangle}$ along the ζ ($\zeta = x, y, z$) axis, for a quantum dot which has various dimension along one axis (z) and fixed dimension along other axes ($L_x = L_y = 100$ Å).

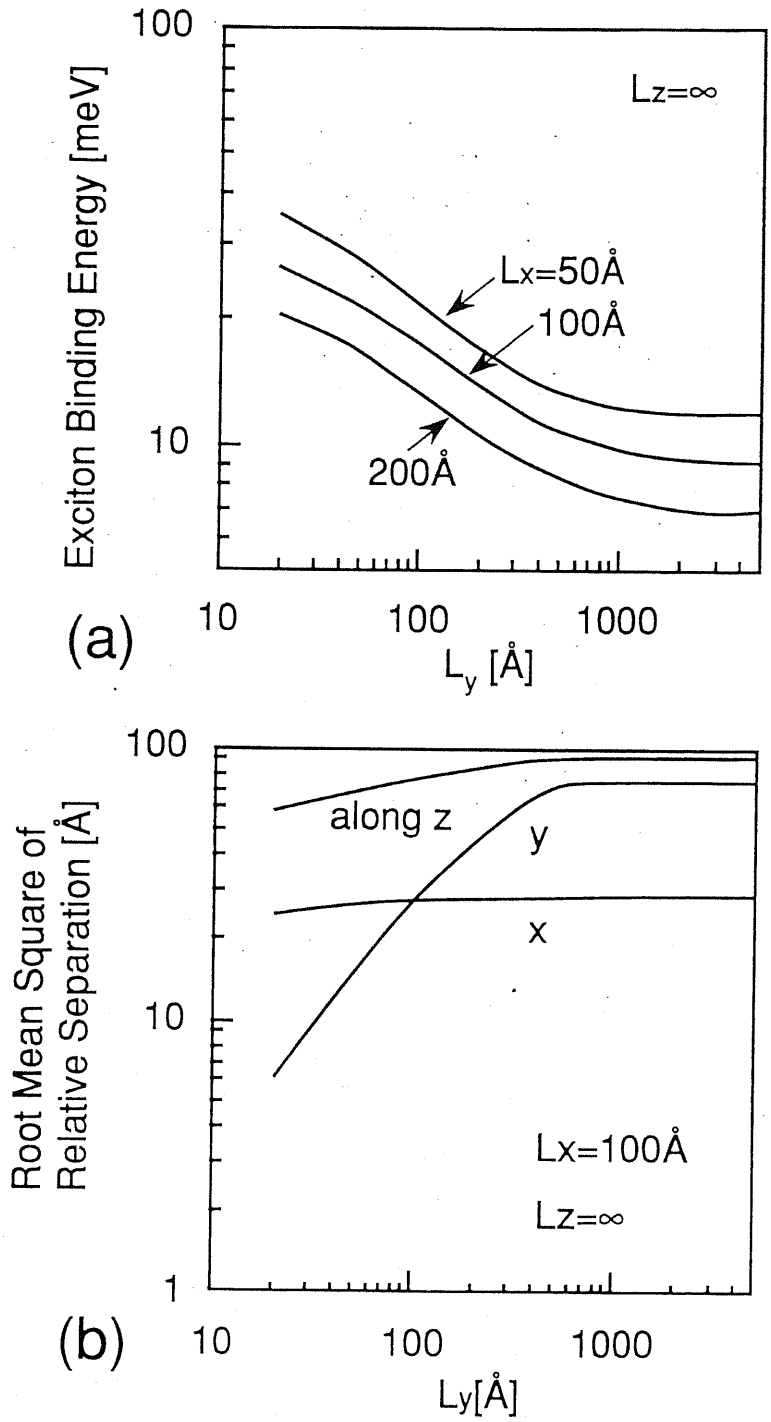

Figure 2.5: a) Exciton binding energy E_C and (b) root mean square of electron-hole separation in the ground state $\sqrt{\langle(\zeta_e - \zeta_h)^2\rangle}$ along the ζ ($\zeta = x, y, z$) axis, a quantum wire which has various dimension along one axis (y) and fixed dimension along other axes ($x = 100$ Å, $z = \infty$).

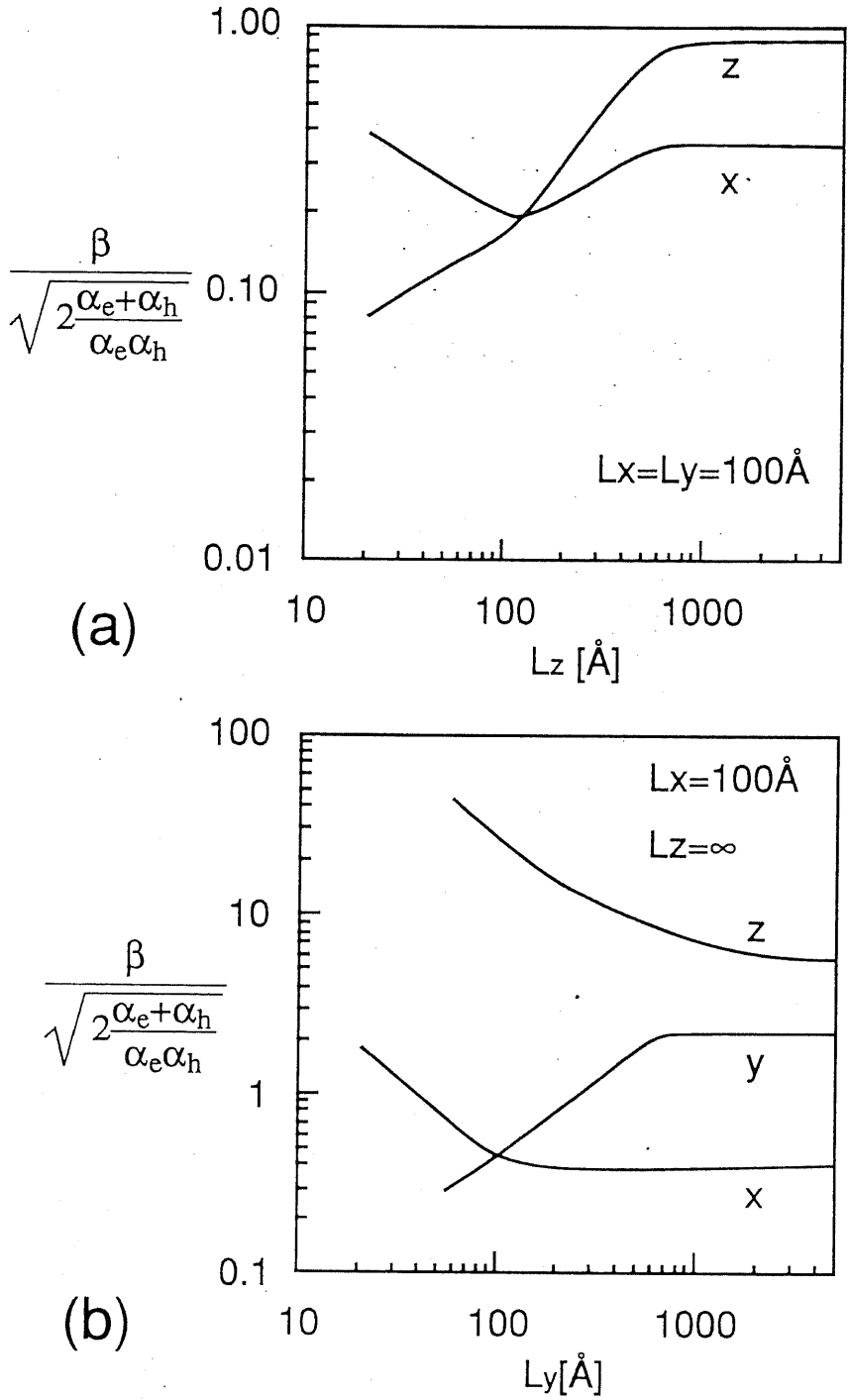

Figure 2.6: Normalized parameter t of Eq. (2.31) in the ground state for (a) a quantum dot which has various dimension along one axis (z) and fixed dimension along other axes ($L_x = L_y = 100$ Å), and for (b) a quantum wire which has various dimension along one axis (y) and fixed dimension along other axes ($x = 100$ Å, $z = \infty$).

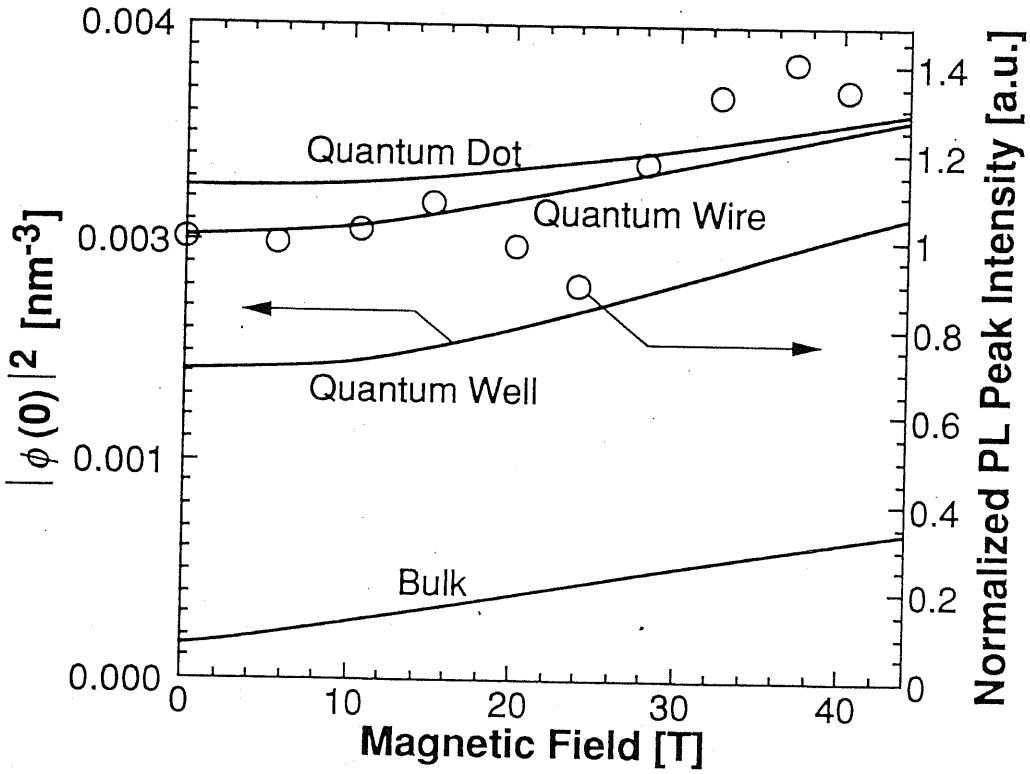

Figure 2.7: Exciton oscillator strength of quantum dot ($L_x = L_y = 16.0$ nm, $L_z = 8.0$ nm), quantum wire ($L_x = \infty$, $L_y = 16.0$ nm, $L_z = 8.0$ nm), and quantum well ($L_z = 8.0$ nm) as a function of external magnetic field along the z axis.

Chapter 3

Structure Dependence of Magnetoexciton Properties in Quantum Wires

abstract

We theoretically study exciton properties of quantum wires (QWRs) with an anisotropic two-dimensional parabolic potential and an rectangular and an triangular shaped cross section in presence of a magnetic field. The calculated results including Coulomb interaction between an electron–hole pair show that the experimental results on magneto-photoluminescence (magneto-PL) of GaAs QWRs can be well explained by this model, demonstrating importance of the exciton effect to understand the magneto-PL properties of QWRs. On the other hand, the change of the exciton binding energy due to the magnetic field is relatively small compared to the total energy shift. Moreover, the results including carrier confinement with an anisotropy or various cross sections show the carrier configuration is strongly depend on the mutual relation of the confinement structure and the applied direction of the magnetic field.

3.1 Introduction

Recently, two dimensional confinement effects of quantum wire (QWR) structures have been observed by many optical measurements such as photoluminescence (PL), photoluminescence excitation (PLE), cathode luminescence (CL) [65, 66] etc. The photoluminescence (PL) peak energy has been found to show clear blueshifts with decreasing lateral width of the QWRs [66]. Optical measurements under external magnetic fields [9–12] have given us much information to characterize carrier confinement in low dimensional structures because we can directly control the confinement of the carriers by the magnetic field. Nagamune *et al.* have reported various magnetophotoluminescence (magneto-PL) measurements of QWRs on those anisotropy [9], the dependence on lateral confinement widths [11], and the dependence on angles of applied magnetic field [64]. Plaut *et al.* have estimated effective mass of QWRs by magneto-PL measurements [10]. In addition, measurement of an anisotropic PL in multi-quantum-well wire structures with lateral width 70-200 nm has been reported [67]. However, most discussions of the magneto-optical properties of QWRs have assumed simplified models for cross sectional shapes of QWRs, i.e. circle or square, or neglecting the Coulomb interaction.

Even though a magnetic field normal to any QWR with a simple structure, a external magnetic field applied to quantum nanostructures yields a condition with a complex anisotropic confinement. In addition, the QWRs used in the experiments have complex nanostructures such as several kinds of cross sections: crescent [65], triangular [66] or arrowhead [68] shapes. Moreover, complex boundary condition of quantum confinement, magnetic field, and electron–hole interactions are all expected

to affect the optical properties of QWRs significantly. Therefore, it is important to include all of those expected mechanisms in the analysis of the spectra.

This chapter theoretically discusses the dependence of magnetoexciton properties on the confinement structures of QWRs. We show calculated results of the magnetoexcitons in the QWRs, i.e. the effect of Coulomb interaction in the presence of a magnetic field and a QWR potential, by the variational method described in the previous chapter. The mutual relation between quantum confinement, magnetic field, and the exciton effect is discussed in detail. Moreover, the dependence of magnetoexciton on the cross section of QWRs and the direction of applied magnetic fields are discussed by a theory using a three dimensional Schrödinger equation. Furthermore, the numerical results for the magneto-PL of QWRs are compared to the experimental results to discuss those anisotropy, the dependence on lateral confinement widths, and the effect from the relation of the structure and the applied magnetic field.

3.2 Anisotropy of Magnetophotoluminescence

Using the variational method presented in chapter 2, the magneto-PL energy in a QW with an anisotropic confinement for three directions of magnetic fields was calculated. Figure 3.1 shows the dependence of (a) the magneto-PL energy calculated with Coulomb force ($E_{e,h,\mathrm{C}} + E_g$), and without Coulomb force ($E_e + E_h + E_g$), and (b) the exciton binding energy E_C of a QWR with an anisotropic 2D parabolic potential on magnetic fields along the different directions, where E_g is the band gap. In this calculation, the following parameters are used: $L_x = 102.5$ Å, $L_y = 198.8$ Å, $m_h = 0.48m_0$, $m_e = 1.42 \times 0.067m_0$, $\varepsilon = 12.8\varepsilon_0$, and $E_g = 1.519$ eV. The experi-

mental results of magneto-PL for the QWRs in Ref. 9 are also shown in Fig. 3.1. It is seen that assuming an electron mass 1.42 times heavier than in bulk GaAs, the magneto-exciton energy $E_{e,h,\mathrm{C}} + E_g$ fits the experimental magneto-PL of the QWRs in Ref. 9. This heavier value of the electron mass is consistent with the theoretical calculation including non–parabolicity of the conduction band, which shows the electron mass of QWRs is heavier than those of bulk by the factor 1.45 [63]. The dimensional parameters $L_x = 102.5$ Å, $L_y = 198.8$ Å are close to the dimensions estimated in Ref. 9 (10 nm and 20 nm). However, the magneto-PL energy calculated without exciton effect $E_e + E_h + E_g$ by the same parameters does not fit the experiments. These results show that our model including the exciton effect well explains the anisotropic magneto-PL, and supports the 2D anisotropic confinement effect in the QWRs. This demonstrates that the exciton effect is important to understand magneto-PL properties.

On the other hand, the relative energy shift due to the magnetic field can be explained without Coulomb interaction. As shown in Fig. 3.1(a), the energy shift is larger for the magnetic fields normal to the direction of weaker confinement (i.e. the energy shift for $\mathbf{B} \parallel x$ is larger than that for $\mathbf{B} \parallel y$, which is again larger than that for $\mathbf{B} \parallel z \parallel$ QWR). The value of the relative energy shift due to the magnetic field is almost same between the calculations with and without Coulomb interaction. These properties are explained as follows. The change of the exciton binding energy and the energy shift by the magnetic field is compared in Fig. 3.1(a) and 3.1(b). At $\mathbf{B} \parallel x$ and $B = 40$ T, the energy shift $E_{e,h,\mathrm{C}}$ increases 17.0 meV compared to $B = 0$, while the exciton binding energy E_{C} increases only 2.2 meV. The change of the exciton binding energy is small (about 13 %) compared to the energy shift due to

the magnetic field. Thus, in the parameter regime of present interest [9] the ground state energy levels of the QWRs in magnetic fields can be understood by the sum of electron/hole single particle energies and the zero-field exciton binding energy.

In summary, The numerical calculations including Coulomb interaction agree with the experimental magneto-PL data of QWRs in Ref. 9 and the results confirms the 2D anisotropic confinement of the QWRs. The exciton effect turns out to be important to determine the magneto-PL in QWRs. On the other hand, the relative energy shift due to the magnetic field can be explained by non-interacting particles, because in the present structures the change of the magneto-exciton binding energy is relatively small compared to the energy shift by the magnetic field. Therefore, the energy level of the QWR in a magnetic field can be understood by the sum of the energy level calculated without Coulomb interaction and the exciton binding energy at the zero magnetic field.

3.3 Magnet-optical effect in GaAs quantum wires with various lateral width

In this section, we discuss theoretical analysis of magnetoexciton properties including a quantum confinement effect in an anisotropic 2D potential, a magnetic field effect, and a Coulomb effect, by the variational method, comparing experimental results of magneto-PL [11].

3.3.1 Experiment

Here we briefly review the magneto-PL measurement for dependence on lateral width of QWs in Ref. 11. The samples of the GaAs/AlGaAs QWRs with various lateral

widths L_w show consistent blueshift of the PL peak with the decrease of the lateral width [66]. The QWR structure has a triangular-shaped cross section, and the ratio of lateral width to the vertical thickness is about two. The direction of the magnetic field is illustrated in Inset of Fig. 3.2.

In Fig. 3.2, the measured PL peak energy of the QWRs [11] is plotted by circles with a dot as a function of the magnetic field B for the various wire widths L_w. The peak of PL spectra shows blueshift with increase of the magnetic field. The energy shift due to the magnetic field becomes smaller with decreasing wire width. This shows enhancement of the lateral confinement in narrower QWRs.

3.3.2 Theoretical analysis

To analyze the experiments, the variational method discussed in Chapter 2 was used. Material parameters except for the electron effective mass m_e^* are assumed by those of bulk GaAs: $m_h{}^* = 0.45m_0$, and $\varepsilon = 12.8\varepsilon_0$, and $E_g = 1.519$ eV. The electron effective mass m_e^* is taken as 1.35 times larger than that of bulk GaAs ($0.067m_0$) in order to take the band mixing effect in a QWR into account [63]. $\omega_{\zeta,j}$ is chosen such as that the ground state single-particle energy is consistent with the experimental dimensions of the QWR observed by scanning tunnel micrometer as shown in Table 3.1.

In Fig. 3.2, the calculated Magneto-PL energy is shown as a function of the magnetic field B by solid lines, comparing to the experiment. This indicates that the calculation agrees well with the experiment, demonstrating that the energy shift is well explained by the effect of 1D excitons confined by a QWR in the magnetic field. The exciton binding energy is estimated as shown in Table. 3.1, which enhances

Table 3.1: Comparison between fitting parameters used in the calculation (this work) and measured values in the experiment (Ref. 11).

Calculation							Experiment	
L_y	$\frac{1}{2}\hbar\omega_{e,x}$	$\frac{1}{2}\hbar\omega_{h,x}$	$\frac{1}{2}\hbar\omega_{e,y}$	$\frac{1}{2}\hbar\omega_{h,y}$	E_{Bind}	E_0	E_0	L_w
(nm)	(meV)						(meV)	(nm)
29.0	4.94	0.93	19.8	3.73	12.0	153.6	153.8	~ 30
20.9	9.52	1.79	38.1	7.17	15.2	156.0	156.1	~ 25
15.9	16.4	3.1	65.8	12.4	18.0	159.9	160.0	~ 15
12.5	26.6	5.0	106.4	20.6	20.9	165.6	165.7	~ 10
9.7	44.2	8.3	176.7	33.3	24.7	175.7	175.7	~ 7

with increasing lateral width.

Note that the theoretical results describe the transform of energy shift configuration from lower to higher magnetic field range. Namely, in the low magnetic field range, the PL peak positions are diamagnetically changed (i.e., the shift is proportional to the square of the magnetic field), while, in the high magnetic field region, the energy shifts of the QWRs change more linearly against the magnetic field than those in the low magnetic field, in the same way as the bulk regarding the Landau level shift. In the experiment, those tendencies are found more clearly in the wider QWRs. The theory accurately describes these properties for the all lateral widths except $L_w = 7$ nm. These results clearly demonstrate that the enhancement of the lateral confinement energy and of the exciton binding energy in the narrower QWRs, considered in the theory, cause the measured magneto-PL properties.

In the case of $L_w = 7$ nm, however, the measured magneto-PL shift is smaller than the calculated shift. In addition, the PL shift due to the magnetic field of $L_w = 7$ nm is measured to be larger than that of $L_w = 10$ nm. This indicates that in the narrower QWR the exciton wavefunction more penetrates from the 2D

potential wells to the barrier with a finite height.

In summary, the theoretical analysis demonstrates that the measured magneto-PL of the QWRs is the result from the enhancement of the lateral confinement energy and of the exciton binding energy in the narrower QWRs. In addition, the analysis found the exciton wavefunction more penetrates from the well region to the barrier region in the narrower QWR.

3.4 Cross shape dependence under varied direction of the magnetic field

This section discusses the effect of the mutual relation between cross sectional shape of a QWR and the direction of an applied magnetic field for the magneto-PL. By this theory, the angle-resolved magneto-PL in triangular-shaped QWRs [64] is analyzed.

3.4.1 Calculation model

Figure 3.3 has illustrated of our model of the quantum wire structure. We assume a quantum wire structure with finite length of $L_z = 800$ Å confined by a barrier of infinite height. The length of QWRs behaves almost same as a QWR with infinite length for the electronic states such as eigenenergies, wavefunctions, and density of states at the near bandedge [57]. We are focusing on the properties under a magnetic field perpendicular to the QWRs. The cross sectional shape is assumed as rectangle or triangle. The three dimensional Shrödinger equation for an single electron is solved by numerical calculation of the finite difference method. The effective mass of $m_e^* = 0.067$ is used.

3.4.2 Results and discussion

Figure 3.4(a) shows ground state energy at magnetic field $B = 50$ T for quantum wire with ground state quantized energy of $E_0 = 35.9$ meV at the zero magnetic field as a function of applied angle of the magnetic field. Insets of Fig. 3.4(a) have illustrated the direction of the magnetic field, where $\theta = 0°$, $90°$ is corresponding to parallel to the x-axis, the y-axis, respectively. In this figure, various ratios of the dimension along the x-axis L_x and y-axis L_y are shown by several lines. In symmetry case along the x- and y-axis, the energy reaches to the maximum at $\theta = 0°$, $90°$ and to the minimum at $\theta = 45°$.

This behavior is more clearly understood by examining wavefunction along the cross section, shown in Fig. 3.5. The wavefunction at the zero field and at $B = 50$ T along the direction $\theta = 0°$ and $90°$ is shown. The directions of the applied magnetic field have been schematically illustrated in Inset. The square-shaped wavefunction at the zero field shrinks along the direction normal to the magnetic field. While this shrinkage is almost same between $\theta = 45°$ and $\theta = 90°$, the shrinkage of wavefunction parallel to the magnetic field depends on the angle θ, where that of $\theta = 90°$ is more shrunk by the confinement potential than that of $\theta = 45°$. As shown, because of the less confinement along the direction of the diagonal line compared to the direction of the side, the enhancement of the energy at $\theta = 90°$ (and $\theta = 0°$) due to the magnetic field is larger than that at $\theta = 45°$. We call this effect a 'corner effect' afterward. The energy change of 1.2 meV between the maximum and the minimum indicates the possibility of experimental detection.

In the much anisotropic rectangular shaped QWR such as 190 Å $\times$ 155 Å and 201 Å $\times$ 150 Å, the energy shift reflects those confinement structures, i.e. the energy

reaches to the maximum (minimum) at the magnetic field normal to the most (less) confined direction $\theta = 0°$ ($\theta = 90°$), respectively.

In the slightly anisotropic case such as 174 Å × 164 Å, the energy behaves the mixture of the two effects corresponding to the freedom along the diagonal and that along the longer side. These behavior are sensitive to the ratio of the two side lengths. As shown above, the magnetic field effect are sensitive to the anisotropy.

The results for the triangular QWR is shown in Fig. 3.4(b). In the equilateral triangular shaped QWR (top angle:60°, bottom: 260 Å), the energy reaches to the minimum at $\theta = 0°$, 60° and the maximum at $\theta = 30$ °, 90°, which reflects the symmetry of the cross section. In contrast to the square case, the energy change between the maximum and the minimum is only 0.2 meV. This indicates that high sensitivity is required to detect the angular dependence or the 'corner effect'.

In Fig. 3.6, the wavefunction in equilateral triangular shaped QWRs along the cross section is shown for the zero field and for $B = 50$ T of $\theta = 0°$ and 90°. $\theta = 0°$ and 90° is the angle which gives the maximum and the minimum energy of the magnetic field, respectively. When the zero field, the wavefunction is found to have round corners. When $B = 50$ T, the wavefunction shrinks more at $\theta = 0°$ which is normal to the side compared to $\theta = 90°$. However, the shrunk effect is merely changed between $\theta = 0°$ and 90° in contrast to that of the square. In other words, the 'corner effect' is very small because of the round shaped wavefunction. This is attributed to the small dependence of the energy on the angle of the magnetic field.

Figure 3.6 also shows the results for triangles with anisotropic sides by several solid lines. This shows the behavior of the angular dependence is affected only the anisotropy because of round shaped wavefunction, in contrast to that of the

rectangular which consists of the anisotropic effect and the 'corner effect'.

A QWR with the other cross sectional shape is expected to have less 'corner effect' than that of the rectangular QWR, since the wavefunction of the rectangular QWR has the most acute angle in the corners than that of others. In addition, the 'corner effect' should be more enhance in the confinement structure of the less height compared to the infinite height assumed here, since the penetration of wavefunction from the well region to the barrier region causes the sharper corner in the wavefunction.

Figure 3.7 describes the calculated result to analyze the measurement of angle-resolved magneto-PL in triangular-shaped GaAs QWRs [64], where the calculation is shown by a solid line. The experiment is shown by open circles with error bars estimated in Ref. 64. The cross sectional shapes assumed in the calculation and that used in experiment are illustrated in Insets. Though the calculation well fits the experiment, the assumed shape has 1.7 times wider lateral dimension than that estimated in the experiment. This is expected to be because of the leakage of wavefunction from experimental QWRs, in spite of the assumption of the infinite barrier in the theory.

In summary, the carrier properties under the varied direction of the applied magnetic field are found to be affected the freedom of the carrier along the corner and along the anisotropic sides in the cross sectional shape of the structures. The carrier configuration under varied direction of the magnetic field sensitively reflects those confinement structures.

3.5 Conclusion

This Chapter theoretically discussed the dependence of magnetoexciton properties on the confinement structures of QWRs. We have numerically calculated the magneto-excitons in the QWRs, i.e. the effect of Coulomb interaction in the presence of a magnetic field and a QWR potential, by the variational method, and discussed the mutual relation of those effects. Moreover, the dependence of magnetoexciton properties on the cross section of QWRs and on the direction of the applied magnetic field are discussed by the theory using a three dimensional Schrödinger equation. Furthermore, the numerical results for the magneto-PL of QWRs were compared to the experimental results and discuss those anisotropy, the dependence on lateral confinement widths, and the dependence on structures and on angles of applied magnetic field.

The numerical calculations including Coulomb interaction and 2D anisotropic confinement agree with the experimental magneto-PL data of QWRs [9,11], which demonstrates that the measured magneto-PL is caused by the 2D confined magnetoexciton effect with the 2D anisotropic confinement and the dependence on lateral width of the QWRs. The exciton effect turns out to be important to determine the magneto-PL in QWRs. On the other hand, the change of the exciton binding energy due to the magnetic field is relatively small compared to the total energy shift. Thus, the energy level of the QWR in a magnetic field can be understood by the sum of the energy level calculated without Coulomb interaction and the exciton binding energy at the zero magnetic field. Moreover, the theoretical results using a three dimensional Schrödinger equation show magnetoexciton properties are very

sensitive to the cross section of QWRs and the direction of applied magnetic fields.

These results clearly demonstrate that the 1D magnetoexciton effect and the confinement structure dependence are important to understand the magneto-optical properties and to estimate the confinement in those structures.

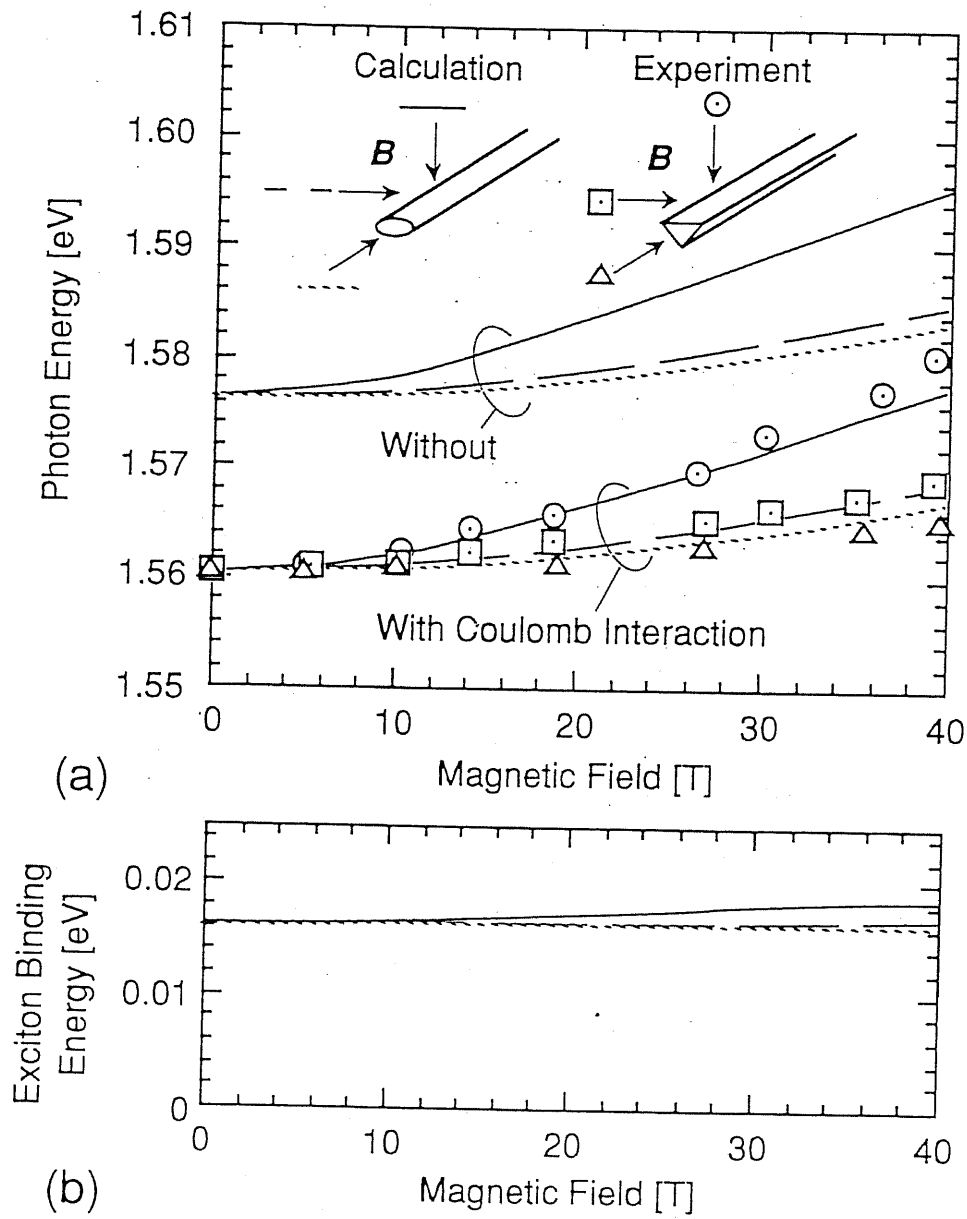

Figure 3.1: (a) Photon energy $E_{e,h,C}+E_g$ (calculated with Coulomb interaction) and $E_e+E_h+E_g$ (without Coulomb interaction), (b) exciton binding energy E_C of a quantum wire with an anisotropic 2D parabolic potential ($L_x = 102.5$ Å, $L_y = 198.8$ Å, $L_z = \infty$) in different direction and magnitude of the magnetic field. Effective masses are taken as $m_h = 0.48m_0$ and $m_e = 1.42 \times 0.067m_0$. Solid, dashed, and dotted lines show the magnetic field along x, y and z, respectively. In (a), experimental magneto-photoluminescence data of the quantum wires in Ref. 9 are shown. Circles, squares, and triangles represent the data for $\mathbf{w} \perp \mathbf{B} \parallel \mathbf{k}$, $\mathbf{w} \perp \mathbf{B} \perp \mathbf{k}$, and $\mathbf{w} \parallel \mathbf{B} \perp \mathbf{k}$, respectively, where $\mathbf{w}$ and $\mathbf{k}$ is a parallel vector to the quantum wires and a perpendicular vector to the substrate, respectively. Inset: Schematic illustrations of the quantum wires and the directions of the magnetic field.

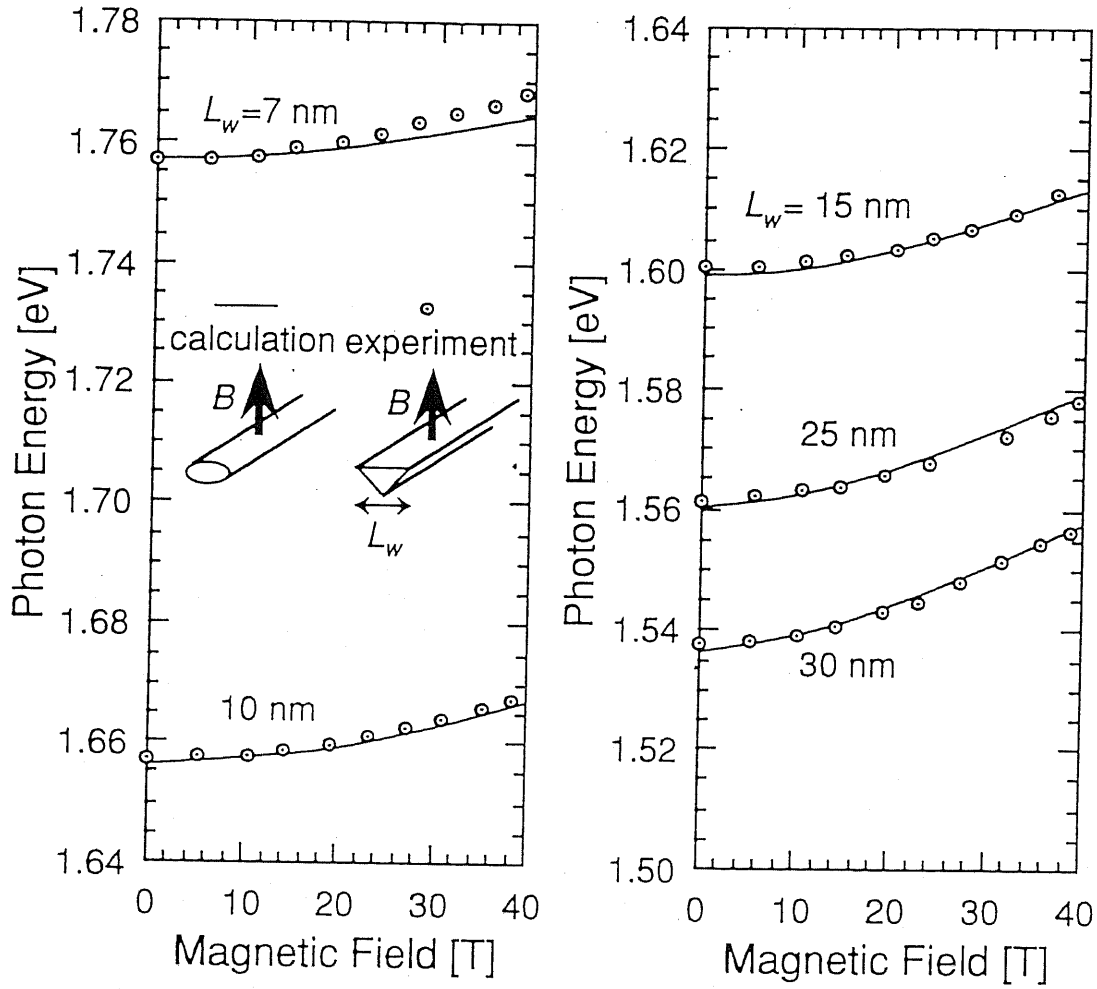

Figure 3.2: Magnetophotoluminescence peak energy with variation of L_w. Experiment (Ref. 9) and calculation (this work) is shown by circles and solid lines, respectively.

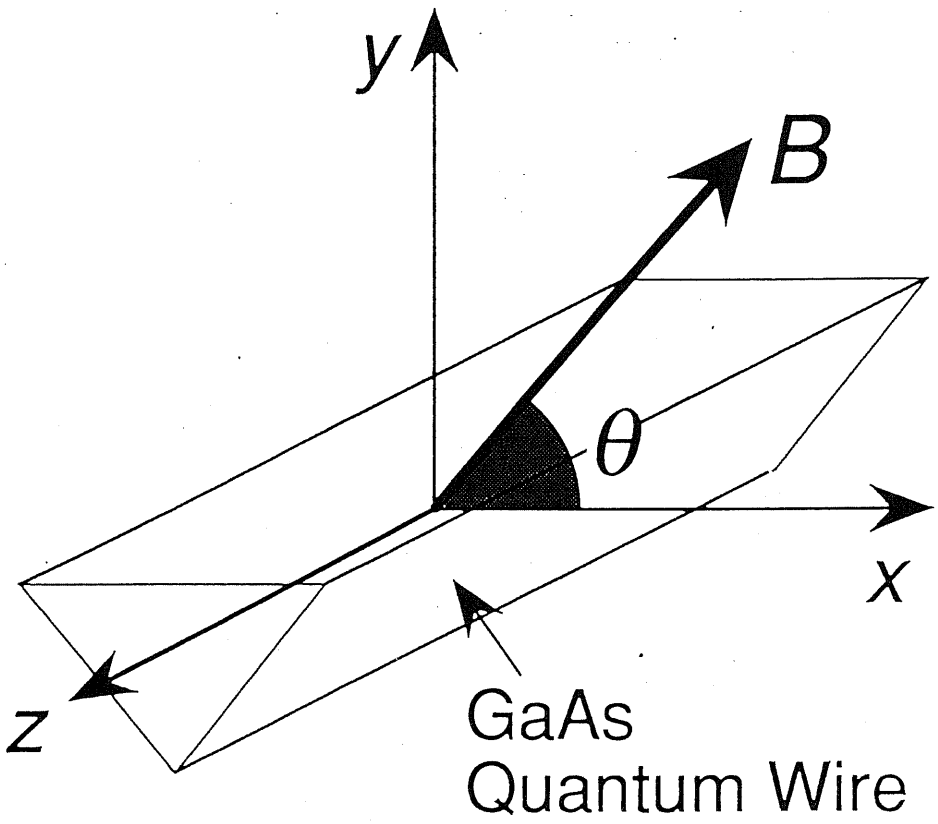

- quantum wire with finite length
- infinite barrier height
- three dimensional Schrödinger equation

Figure 3.3: Model of quantum wire with any cross sectional shape.

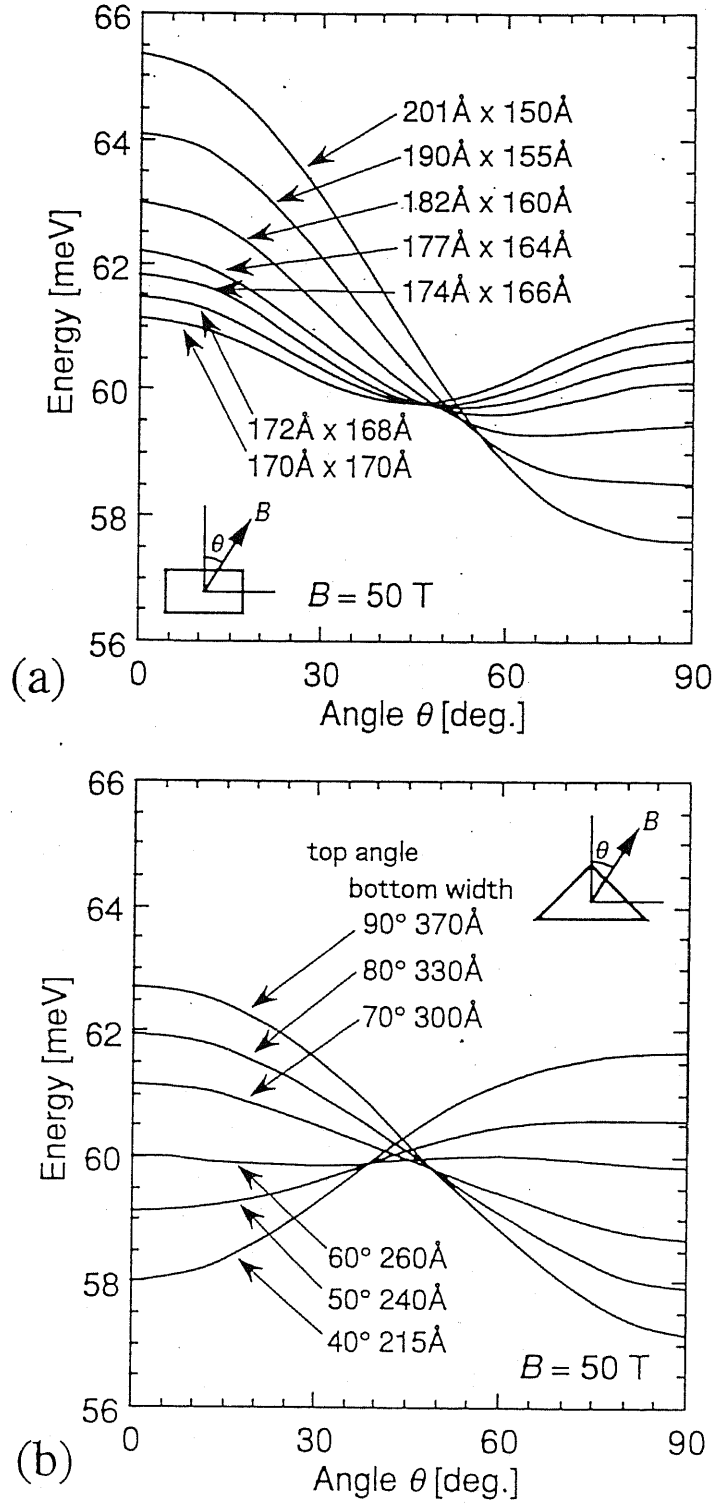

Figure 3.4: Ground state energy of electron in quantum wire with various (a) rectangular and (b) triangular shaped cross section as a function of applied angle of magnetic field. Inset: Schematic illustration of the cross sectional shape and applied magnetic field.

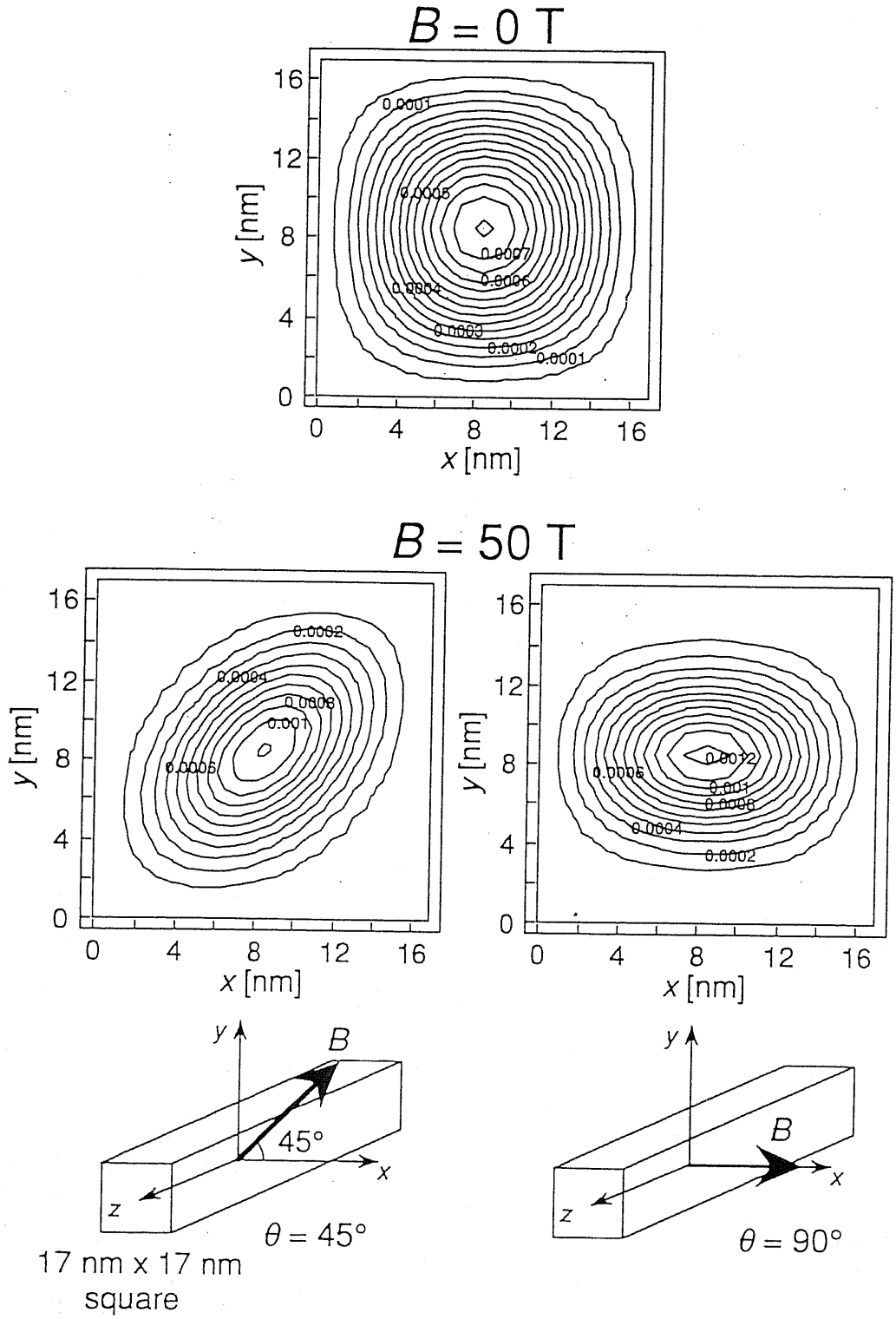

Figure 3.5: Wavefunction of ground state electron in quantum wire with square shaped cross section with and without applied magnetic field. The direction of the magnetic field is illustrated in Inset.

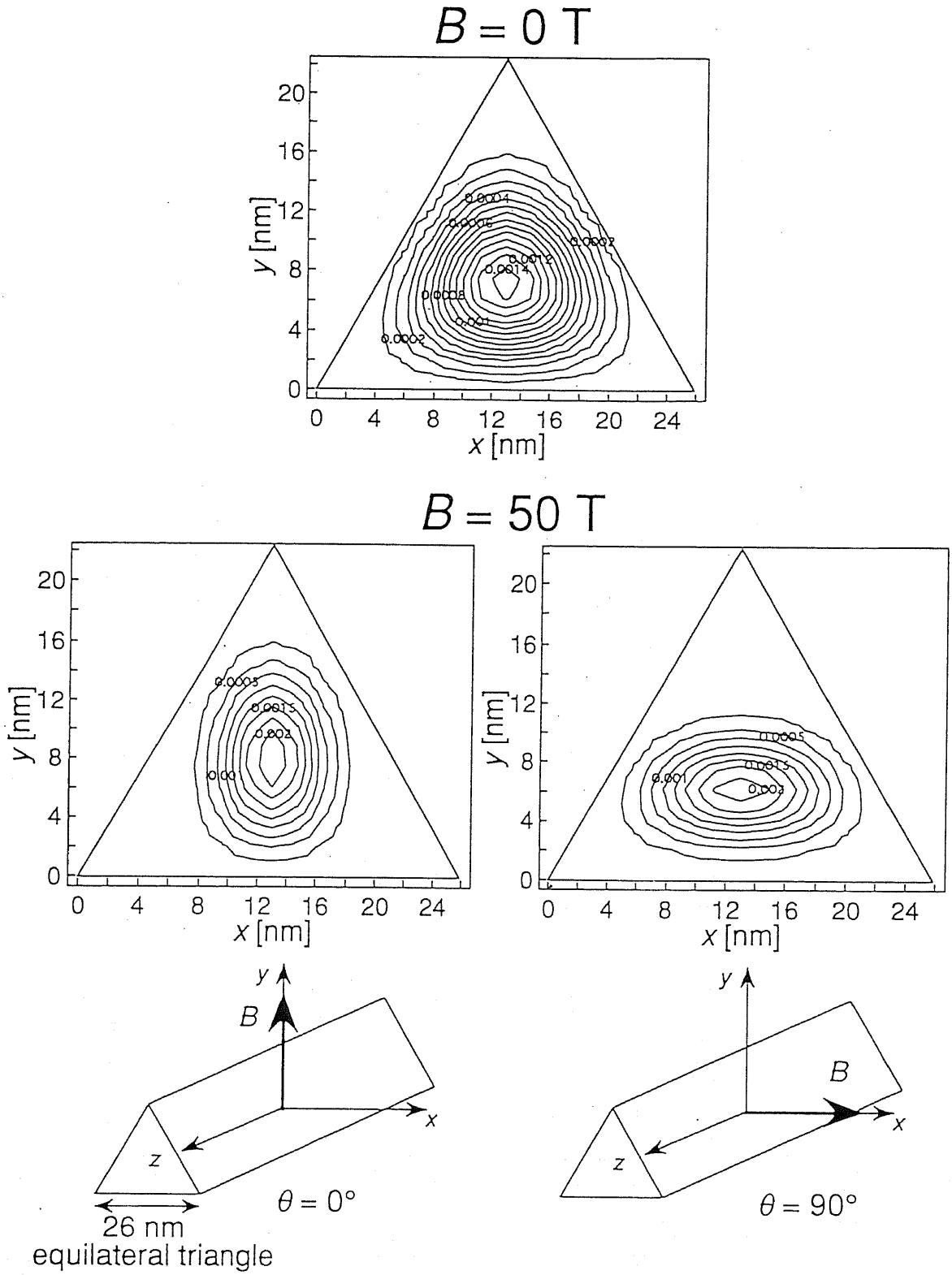

Figure 3.6: Wavefunction of ground state electron in quantum wire with equilateral triangular shaped cross section with and without applied magnetic field. The direction of the magnetic field is illustrated in Inset.

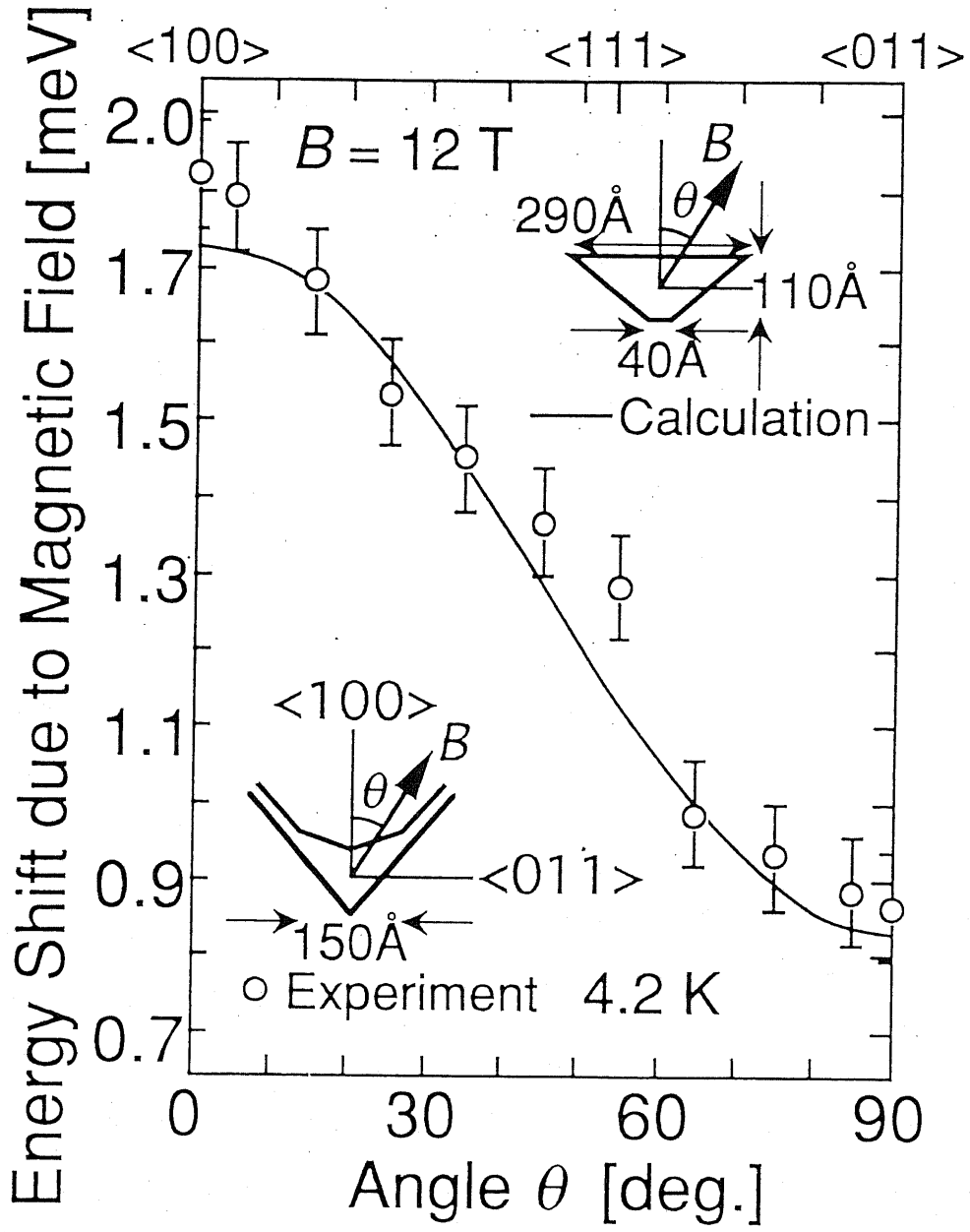

Figure 3.7: Magnetophotoluminescence energy as a function of applied angle of magnetic field. Circles show experiment for quantum wire with triangular cross section [64]. Inset: Schematic illustration of the cross sectional shape and applied magnetic field.

Chapter 4

Photon–Magnetoexciton Interaction in Microcavities with Quantum Wells

abstract

Exciton-polariton mode splitting of quantum wells (QWs) in microcavity is investigated under a high magnetic field up to $B = 14.5$ T. The magnetic field dependence of the splitting interval has been measured for the precisely tuned photon and exciton mode. The comparison between a different number of QWs for the mode splitting is also discussed. Enhancement of the splitting interval with increase of the magnetic field has been found, which shows enhancement of magnetoexciton–photon interaction. Theoretical analysis demonstrates these properties are mainly caused by the increase of exciton oscillator strength due to the magnetic field, and also suggests cavity effect on these properties.

4.1 Introduction

The controlled spontaneous emission in semiconductor microcavities has been widely studied to verify cavity quantum electrodynamics and to improve the performance of optical devices [30]. Lifetimes of excitons in quantum wells embedded in microcavity (QWMC) are expected to be controlled by the cavity effect because of strongly coupling with photon mode in the cavity. In order to clarify those properties, proper understanding of photon–exciton interaction is important.

Moreover, the strong coupling of excitons and photons in the structure with QWMC causes normal mode splitting of exciton-polariton, which is equivalent to vacuum-field Rabi splitting (VRS) in atom-cavity system [41]. In addition, the coherent exciton-polariton emission with oscillation from resonantly excited excitons in a microcavity has been demonstrated [42,43], which is equivalent to the vacuum-field Rabi oscillation. Recently, the properties of exciton-polariton mode are intensively investigated from various aspects: dependence on temperature [44–46], on electric field [44], on magnetic field [47], on excitation power [43,48], on number of quantum wells (QWs) [49,50], on angle of emission [51] etc. and also controlled spontaneous emission [52]. These properties have been obtained by a quantum mechanical theory with Green function [53], and also with a model of a photon-exciton-coupled state, called 'dressed exciton', which has reversible spontaneous emission [54–56].

Tignon *et al.* [47] have reported the exciton–polariton mode splitting in a magnetic field applied normal to QWs embedded in a microcavity. They have showed enhancement of splitting interval due to the magnetic field, obtaining the enhancement of interactions between exciton and cavity photon. However, their data which

have a finite detuning between exciton and photon mode are not sufficient to quantitatively discuss photon magnetoexciton interaction.

The external magnetic field effect on the interaction between photon-exciton interaction is important since the magnetic field can directly and continuously control the parameter of exciton mode such as wavefunction, oscillator strength, remaining the parameter of cavity photon mode. Hence, the interaction between photon and exciton can be examined under the control of exciton only. Moreover, the high magnetic field up to 15 T normal to QWs causes strong lateral confinement of carriers by cyclotron motion, which makes magnetoexciton state and can consider as QDs. It enables us to clarify the electromagnetic field effects of the cavity on magnetoexciton and also to predict the cavity effect on exciton in QDs.

In this chapter, we report the measurements of the exciton–polariton mode splitting under a high magnetic field up to 14.5 T. The dependence of the strength of interaction between magnetoexciton and photon on the magnetic field is presented. The effect of cavity on oscillator strength of magnetoexciton is also discussed. Moreover, the mode splitting is analysed by a theory on the basis of a variational method for magnetoexciton oscillator strength, and of the transfer matrix method for reflectivity spectra. In addition, the effect of the number of QWs embedded in the microcavity on the splitting is discussed.

4.2 Magneto-optical measurement of exciton-polariton mode splitting

In following, the measurement of exciton–polariton mode splitting of QWMC in the high magnetic field up to the 14.5 T is shown. Figure 4.1 shows the schematic

illustration of the sample used in our experiments. The samples were grown on a GaAs substrate by the low-pressure MOCVD system [49]. They include 76-Å-thick GaAs multiple QWs with 100-Å-thick $Al_{0.2}Ga_{0.8}As$ barriers, which are located at center of an $Al_{0.2}Ga_{0.8}As$ λ-microcavity. Two samples with 5 QWs and 13 QWs are used for the measurements. The optical microcavity is sandwiched between two distributed Bragg reflector (DBR) mirrors with 25 (on the substrate) and 33.5 (on the air) pairs of $AlAs/Al_{0.4}Ga_{0.6}As$. The peak reflectivity of each DBR of the samples is about 99.9 %. Because of the nonuniformity of epitaxial growth, the resonant wavelength of the microcavity can slightly and continuously vary with minute displacement of a probing position on the wafer while the thickness of QW changes hardly. The thickness fluctuation of a QW is less than one monolayer due to a short growth time. For a typical substrate with dimension 20×20 mm^2, a two percent change of growth rate was observed between the center and the edge of the sample. A two percent change of thickness causes a two percent change of the resonant wavelength of the microcavity, while the QW exciton energy is hardly changed since the exciton energy is mainly corresponding to the GaAs band gap. A micro-positioning actuator with optical fibers was used to continuously change the probing point on the wafer for finding the tuned and/or detuned position between the resonance wavelength of the microcavity and the PL peak wavelength of QW excitons.

4.2.1 Experimental setup for magneto-optical measurements

The experimental setup for the magneto-optical measurements is illustrated in Fig. 4.2. Incident light from white light source of Halogen was induced by an optical fiber

to the sample in superconducting magnet system. The sample was cooled to 30 K with the thermocontroller. A magnetic field up to 14.5 T was applied normal to QW plane. The signal light was induced by another optical fiber to the detector of optical multi-channel analyzer system. The edges of the two optical fibers for the sample were held by a micro-positioning actuator with an angle 8° and kept a 600 μm distance to the sample. The incident and reflected angle was 4°. The actuator consists of a $\sim$ 1 m length shaft, a ball bearing, and a x-y translation stage as shown in Fig. 4.2.

4.2.2 Reflectivity spectra

A typical measured reflectivity spectrum by the setup with the two micro-positioning optical fibers is shown in Fig. 4.3, where the QWMC sample with 5 QWs was measured at 77 K. In this figure, clearly splitted double dips which are corresponding to the two blanch of exciton-polariton mode is found at 790.2 nm (1569.0 meV) and 793.6 nm (1562.2 meV). In this measurement, cavity photon mode and QW exciton mode were slightly detuned by controlling the cavity length.

A typical experimental recording of reflectivity spectra under various magnetic field at a fixed probing point is shown in Fig. 4.4, where the QWMC sample with 5 QWs was measured at 30 K. At zero field, the double dips corresponding to exciton-polariton mode are found at 788.1 nm (1573.1 meV) and 791.0 nm (1567.4 meV). These double dips show blueshifts with increase of magnetic field. In the low magnetic field range ($B \lesssim 5$ T), the depth of the dip at shorter wavelength was larger than that of longer wavelength, so that the dip at longer (shorter) wavelength is assigned to an exciton-like mode (a photon-like mode), respectively.

In the high magnetic field range ($B \gtrsim 10$ T), in contrast, the depth of the longer wavelength was smaller than that of the shorter, where the exciton-like mode was at shorter than the photon-like mode. In Fig. 4.4, the assignment of exciton-like mode and photon-like mode is denoted by filled and open allows, respectively.

Between those two ranges (5 T $\lesssim B \lesssim 10$ T), continuous tuning-detuning of exciton and photon mode by the applied magnetic field was realized for the first time. In the middle field range, clear anticrossing behavior between the exciton-like mode and the photon-like mode is found. This shows strong coupling of photons and magnetoexcitons causes the vacuum-field Rabi splitting.

The 11.5 meV shift of the exciton-like mode from the zero field to 14.5 T is explained as follows. The exciton-like mode is expected to shift off the resonant frequency $\approx$ 788.7 nm (1572.0 meV) from the non-interacting exciton mode due to the repulsion between exciton-like mode and photon-like mode. Thus, the shift of the exciton-like mode includes two effects: the energy shift of non-interacting excitons due to the magnetic field, and the repulsion due to the resonance. The former effect is corresponding to the diamagnetic energy shift of excitons in normal QWs without cavity. $GaAs/Al_{0.15}Ga_{0.85}As$ QWs of 65 Å is estimated to have diamagnetic shift of about 7 meV from the zero field to 15 T from the previous magneto-optical experiment [69] and also from the theory mentioned afterward. The latter effect can estimate by the repulsion effect on the photon-like mode from the center of the resonance. Figure 4.4 shows the exciton like mode at zero field (788.1 nm) and at 14.5 T (790.0nm) is repulsed about 3 meV from the center of resonance 788.7 nm (1572.0 meV). Thus, the sum of two effect deduces 10 meV shift of exciton-like mode corresponding to the measurement.

4.2.3 Energy shift of exciton-polariton mode

The reflectivity dip energies of the two modes of exciton-polariton for the 13 QWs' sample are plotted as a function of magnetic field in Fig. 4.5. The marks (open circles, filled squares, open triangles, filled circles) are corresponding to the different cavity length at each probed position. Arrows show the condition where exciton and photon mode are tuned on resonance. As shown in this figure, the tuned energy position, as well as the double dips, shows blueshift with increase of magnetic field. The center of two dips on resonant is found to shift about 7 meV from the zero field to 14.5 T, which is equivalent to diamagnetic energy shift of QWs without cavity. The figure shows the enhancement of the splitting intervals with increasing magnetic field for the tuned and also slightly detuned exciton and photon.

4.2.4 Mode splitting intervals

Figure 4.6 shows energy interval of the magnetoexciton polariton mode splitting as a function of the magnetic field for the QWMC samples with 5 and 13 QWs. Note these data were measured with careful tuning of cavity photon energy to the exciton energy by minute change of the cavity length at each magnetic field in order to accurately measure the effect of the interaction between photons and excitons. In Fig. 4.6, open circles show the data of three layers of InGaAs QWs in a GaAs λ-microcavity by Tignon *et al.*, which have been measured with a finite detuning as mentioned in their report [47]. The finite detuning is expected to enlarge those splitting intervals from the intrinsic splitting of resonant magnetoexciton–polariton mode. In fact, the increase of mode splitting intervals due to magnetic field presented by them is too large to be interpreted by the enhancement of photon–exciton

interaction.

4.3 Theoretical analysis

To analyze the mode splitting intervals, we assume a model on the basis of the transfer matrix analysis method for reflectivity spectra and the variational method for exciton oscillator strength. A detailed theory is shown as follows.

We used the standard transfer matrix analysis method [70] to calculate reflectivity spectra including an exciton absorption dependent on angular frequency ω in the QW layers and a constant absorption at the other layers. For exciton absorption in the QW layers, we assume complex relative dielectric function $\epsilon(\omega) = \epsilon_\infty + \epsilon_r(\omega) - i\epsilon_i(\omega)$, where ϵ_∞ is relative dielectric constant far from the resonant frequency, $\epsilon_r(\omega)$ and $\epsilon_i(\omega)$ is the real and imaginary part which depends on the frequency ω, respectively. For the imaginary part $\epsilon_i(\omega)$, Lorentzian function dependent on frequency is assumed. The real part $\epsilon_r(\omega)$ is derived with the Kramers-Kronig relation from the imaginary part $\epsilon_i(\omega)$. Complex refractive index $n(\omega) = n_\infty + n_r(\omega) - in_i(\omega)$ is derived from the relation $n(\omega) = \sqrt{\epsilon(\omega)}$ since magnetic permeability is $\mu = 1$. Absorption coefficient $\alpha_{\mathrm{QW}}(\omega)$ in the QW layers is $\alpha_{\mathrm{QW}}(\omega) = 2\omega n_i(\omega)/c$, where c is the speed of light in vacuum. Figure 4.7 shows calculated results of mode splitting interval for the QWMC as a function of peak exciton absorption and full width at half maximum of exciton absorption. The used parameters of the QWMC structure are designed values in the samples of the experiments.

For the calculation of magnetoexciton oscillator strength, we use the following variational method simplified compared to that of Chapter 2. Only the relative

motion is included in the analysis. The Hamiltonian of an electron–hole pair with Coulomb interaction is described by

$$\mathscr{H}_{r,\mathrm{C}} = \mathscr{H}_r + \mathscr{H}_{\mathrm{C}}, \tag{4.1}$$

where $\mathscr{H}_{\mathrm{C}} = -e/4\pi\varepsilon r$, $r = \sqrt{r_x^2 + r_y^2 + r_z^2}$, ε is the permittivity, and $\mathscr{H}_r$ is the Hamiltonian of a relative motion of the electron–hole pair. QWs are assumed to be defined by a parabolic confinement potential along the z direction. The single–particle Hamiltonian $\mathscr{H}(x,y)_r^{(x,y)}$ along (r_x, r_y) plane of the structure in a magnetic field along z axis is then

$$\mathscr{H}_r^{(x,y)} = \frac{(\mathbf{P}_r + q\mathbf{A}_r)^2}{2{m_r}^*}, \tag{4.2}$$

where m_r is exciton reduced effective mass.

We assume a variational function of the form

$$\Psi_{r,\mathrm{C}} = \exp\left(-\alpha\left({r_x}^2 + {r_y}^2\right) - \gamma {r_z}^2 - \beta r\right), \tag{4.3}$$

where α, β are variational parameters. To simplify, the wavefunction along the z axis is fixed to $\exp(\gamma {r_z}^2)$. We assumed the ground state of a single harmonic oscillator in parabolic confinement $m_r^*\omega_{rz}^2 r_z^2/2$, with the energy $E_z = \hbar\omega_{rz}/2$, and the wavefunction $\exp\left(-(m_r^*\omega_{rz}r_z^2)/(2\hbar)\right)$.

The results of calculation is shown in Fig. 4.6, where the following parameters were used: peak absorption at the center of the spectrum is $\alpha(\omega_0)$ =5.4 cm^{-1}, full width at half maximum of $\epsilon_i(\omega)$ is $\delta_{\mathrm{QW}} = 3$ meV, $m_r^* = 0.04m_0$, and $E_z = 40$ meV. As shown in Fig. 4.6, the results of the calculation well fits the experiment. This result demonstrates the enhancement of the mode splitting due to the magnetic field is clearly explained by the enhancement of exciton oscillator strength because

of shrinkage of wavefunction due to the magnetic field. From the calculated result, the oscillator strength at 14.5 T is estimated to be 2.2 times as great as that at zero field. In addition, this estimation is equivalent to that from the relation between the mode splitting interval Ω and exciton oscillator strength f: $\Omega \propto \sqrt{f}$ deduced from a simple approximation [71].

While the assumed exciton reduced effective mass of $m_r^* = 0.04m_0$ is equivalent to that reported in Ref. 72 ($0.04m_0$) and in Ref. 73 ($0.042m_0$), the other works have determined the even larger mass such as $m_r^* = 0.05m_0$ [69], $0.069m_0 \lesssim m_r^* \lesssim 0.084m_0$ [74, 75], and $m_r^* = 0.045m_0$ [76] by magneto-optical measurements. If we assume the even larger mass, the enhancement of oscillator strength due to the magnetic field should be smaller compared to that of the above estimation. This assumption induces the possibility that the cavity electromagnetic field enhances the interaction of magnetoexciton and photon in the high magnetic field range.

4.4 Conclusion

In this Chapter, magnetic field dependence of vacuum-field Rabi splitting of exciton-polariton mode for quantum wells (QWs) embedded in microcavity was investigated under the high magnetic field up to $B = 14.5$ T. The magnetic field dependence of the mode splitting interval of the precisely tuned photon and exciton mode has been measured. Moreover, the mode splitting has been analysed by the theory based on the variational method for magnetoexciton oscillator strength, and on the transfer matrix method for reflectivity spectra. In addition, on those effects, the different number of QWs (5 QWs and 13 QWs) embedded in microcavity were compared. The effect of cavity on oscillator strength of magnetoexciton was also discussed.

Continuous tuning-detuning of exciton and photon mode by applied magnetic field was realized, where anticrossing behavior was clearly found. It is found the enhancement of the splitting interval with increase of magnetic field, showing the enhancement of magnetoexciton–photon interaction.

Moreover, the experimental results of the samples with 5 QWs and also with 13 QWs are well explained by the theoretical calculation assuming the reduced effective mass of $m_r^* = 0.04m_0$ for an exciton. This shows the enhanced mode splitting interval is mainly caused by the increase of exciton oscillator strength due to the magnetic field. The oscillator strength at 14.5 T is estimated to be 2.2 times as great as that at zero field. In addition, the large enhancement of the oscillator strength shows the possibility of the cavity electromagnetic field effect on the magnetoexciton.

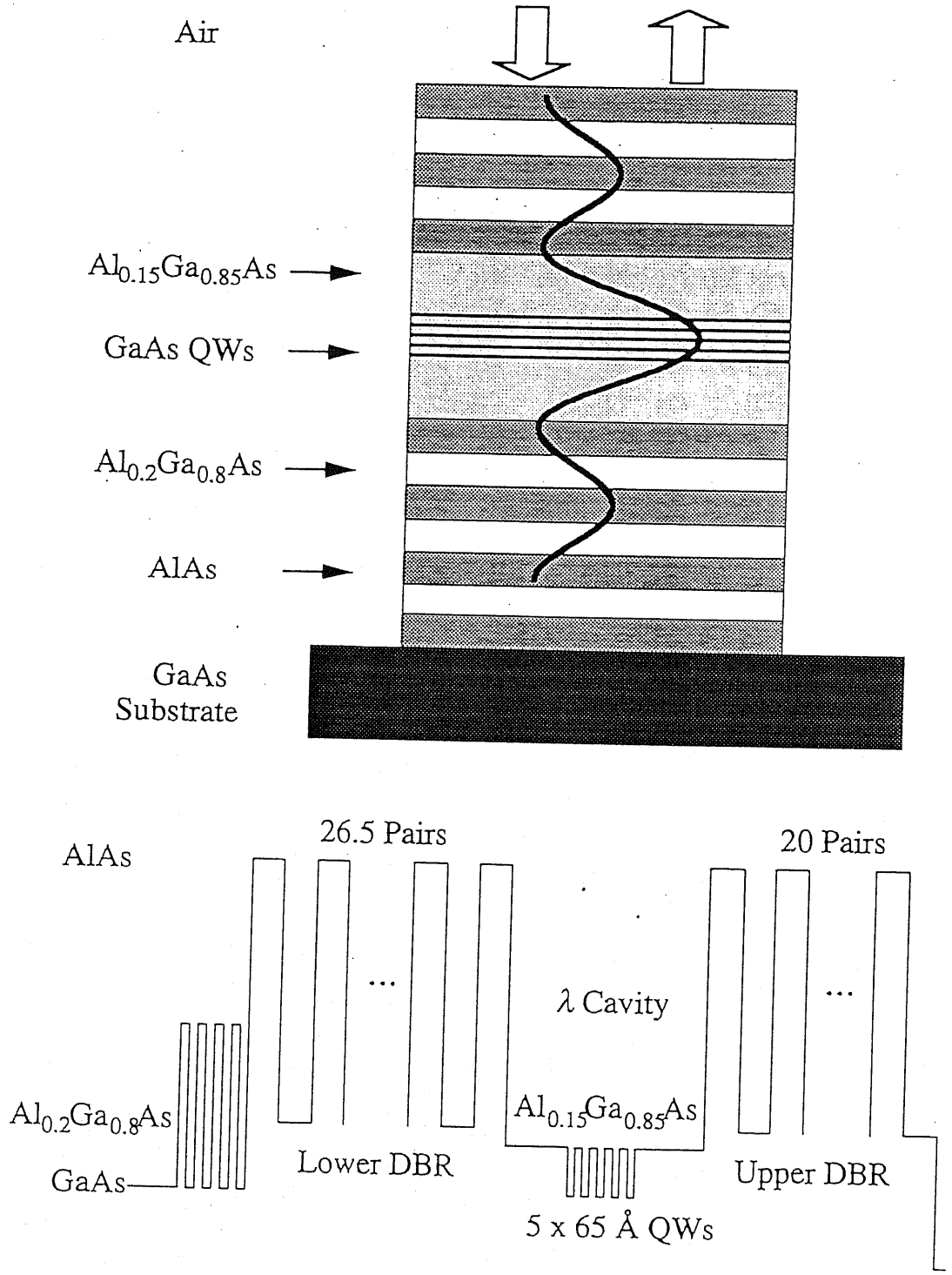

Figure 4.1: Schematic illustration of a λ microcavity with 20/26.5 pairs $AlAs/Al_{0.2}Ga_{0.8}As$ distributed Bragg reflectors and five 65 Å $GaAs/Al_{0.15}Ga_{0.85}As$ quantum wells at the center of the cavity.

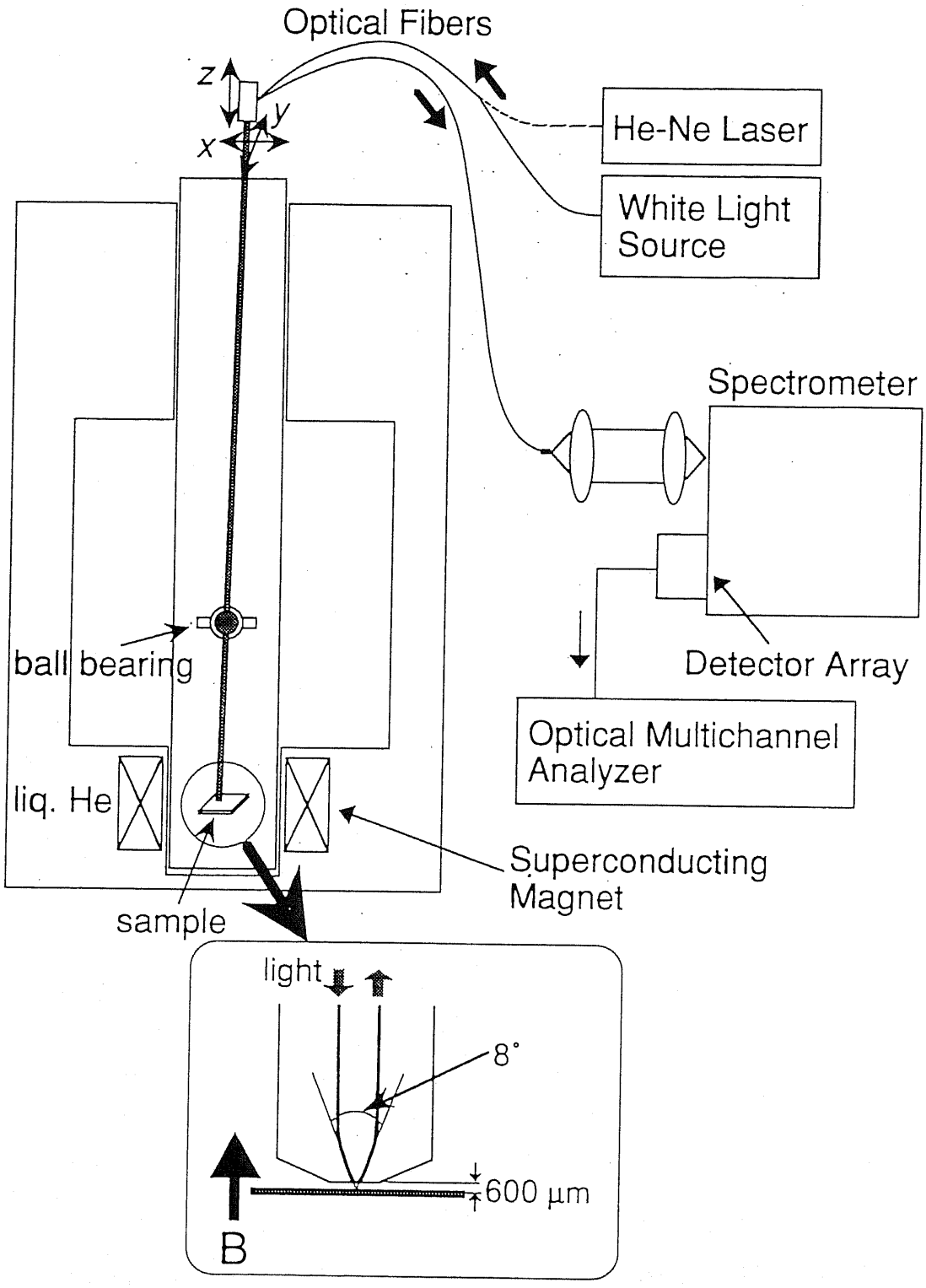

Figure 4.2: Experimental setup for reflectivity and photoluminescence under high magnetic field.

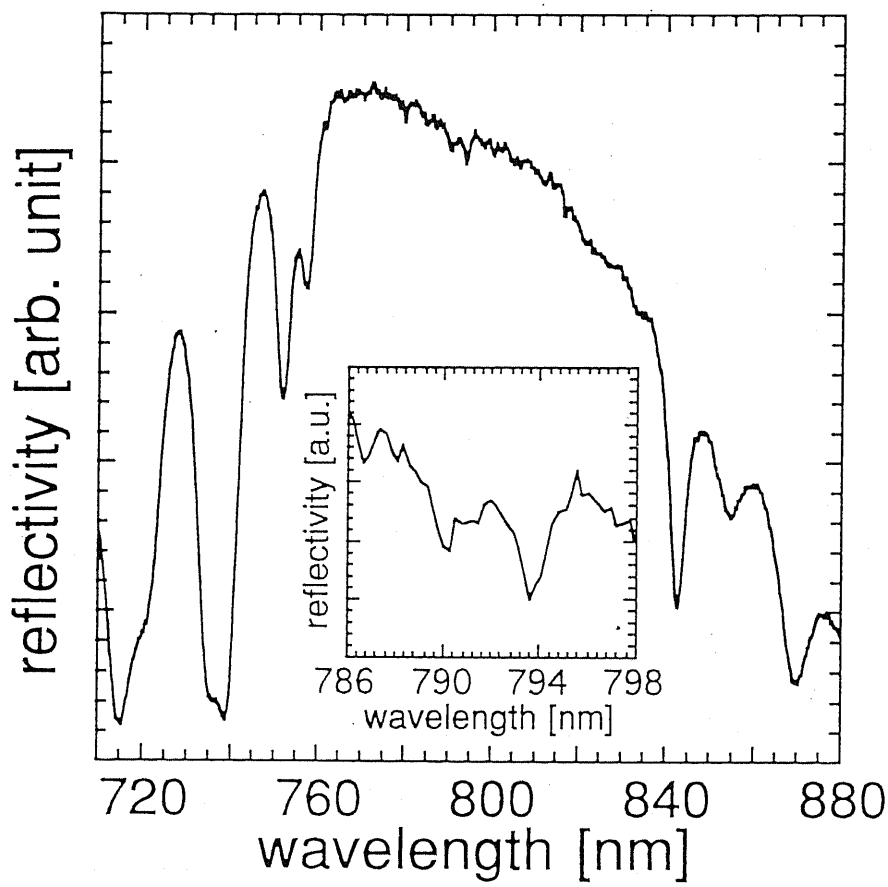

Figure 4.3: Reflectivity spectrum of the structure with 5 quantum wells embedded in microcavity measured at 15 K. For the measurement, cavity photon mode and QW exciton mode was slightly detuned by controlling the cavity length.

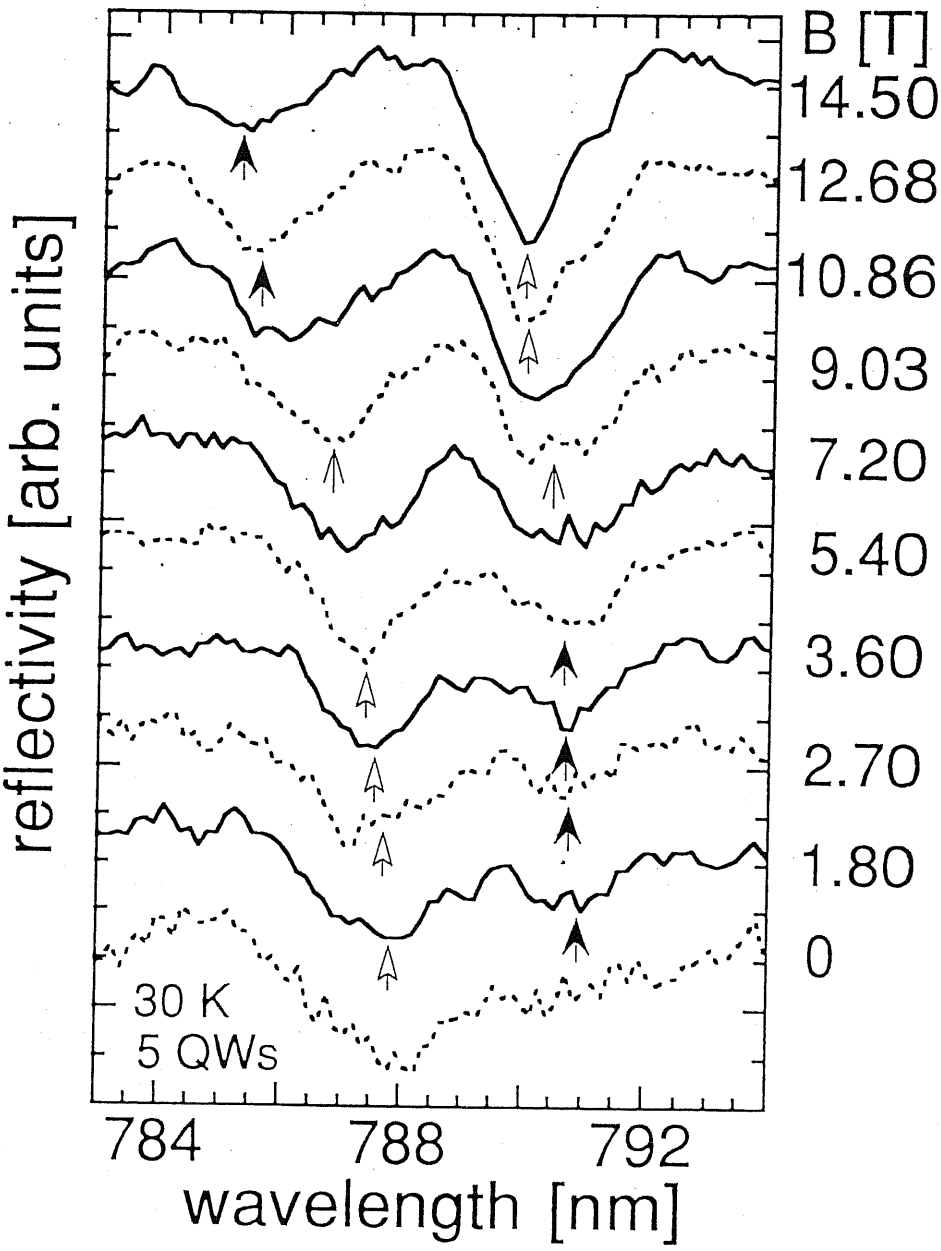

Figure 4.4: Reflectivity spectra of structure of 5 quantum wells embedded in microcavity under various magnetic field at 30 K. Arrows are corresponding to two branches of exciton-polariton mode. Open and filled arrows indicate the photon-like mode and the exciton-like mode, respectively.

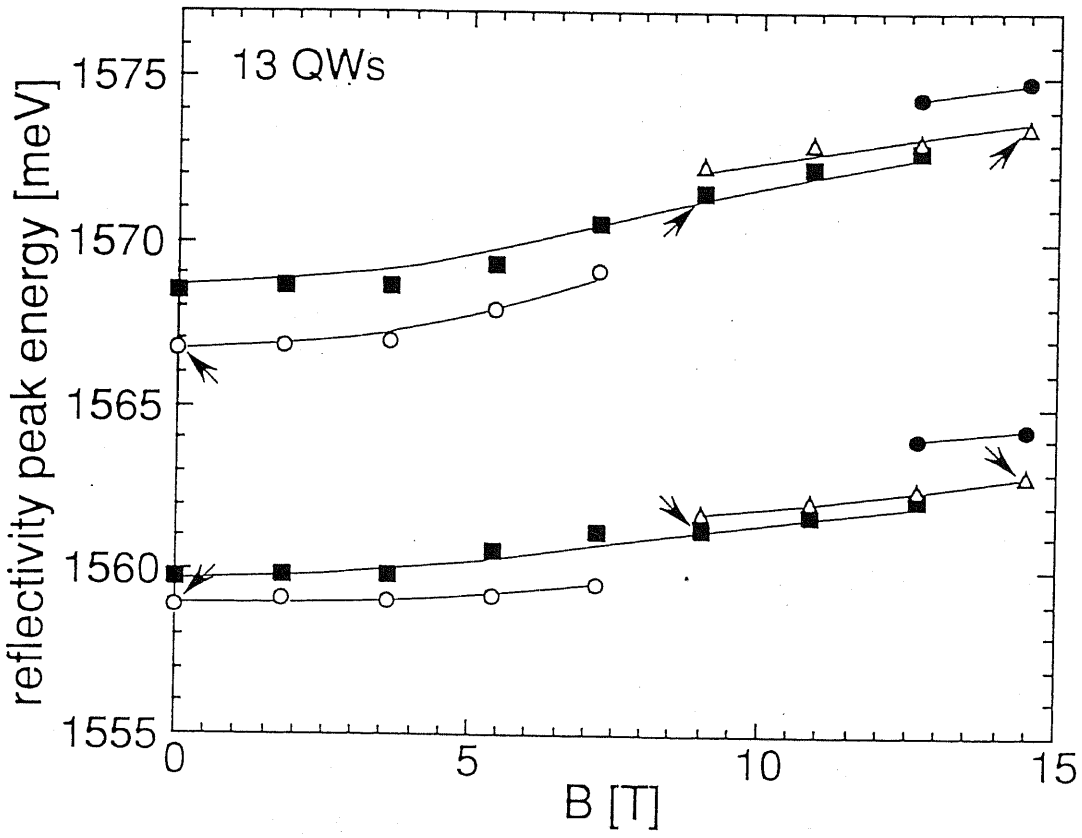

Figure 4.5: Reflectivity peak energy of structure of 13 quantum wells embedded in microcavity as a function of magnetic field. The marks (open circles, filled squares, open triangles, filled circles) are corresponding to the different cavity length. Arrows show the condition where exciton and photon mode are tuned on resonance.

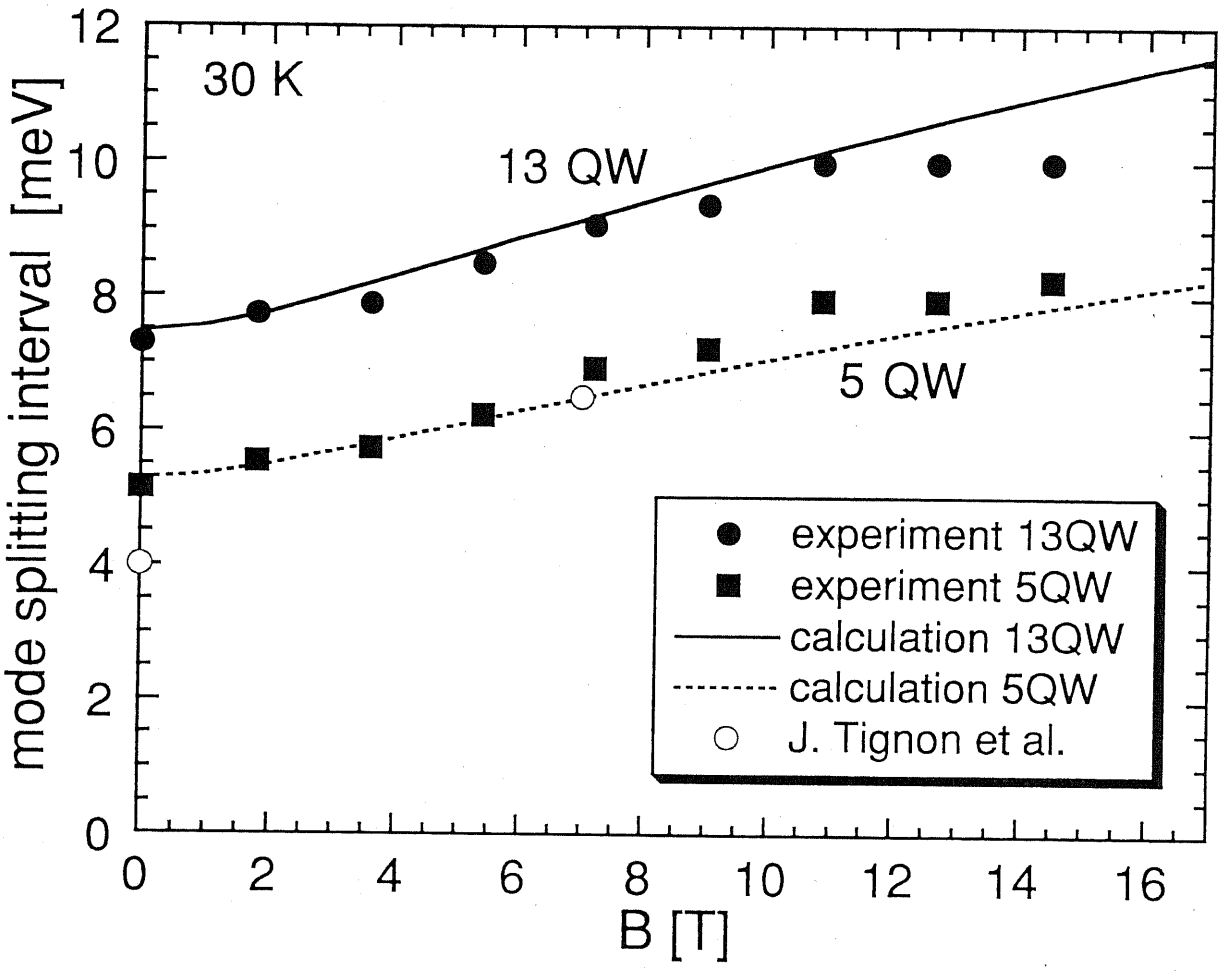

Figure 4.6: Energy interval of exciton polariton mode splitting at tuning positions as a function of the magnetic field for the microcavity with 5 and 13 QWs, shown filled squares and filled circles respectively. Open circles show the data of three layers of InGaAs quantum wells in GaAs λ-microcavity by Tignon *et al.* [47], which have a finite detuning.

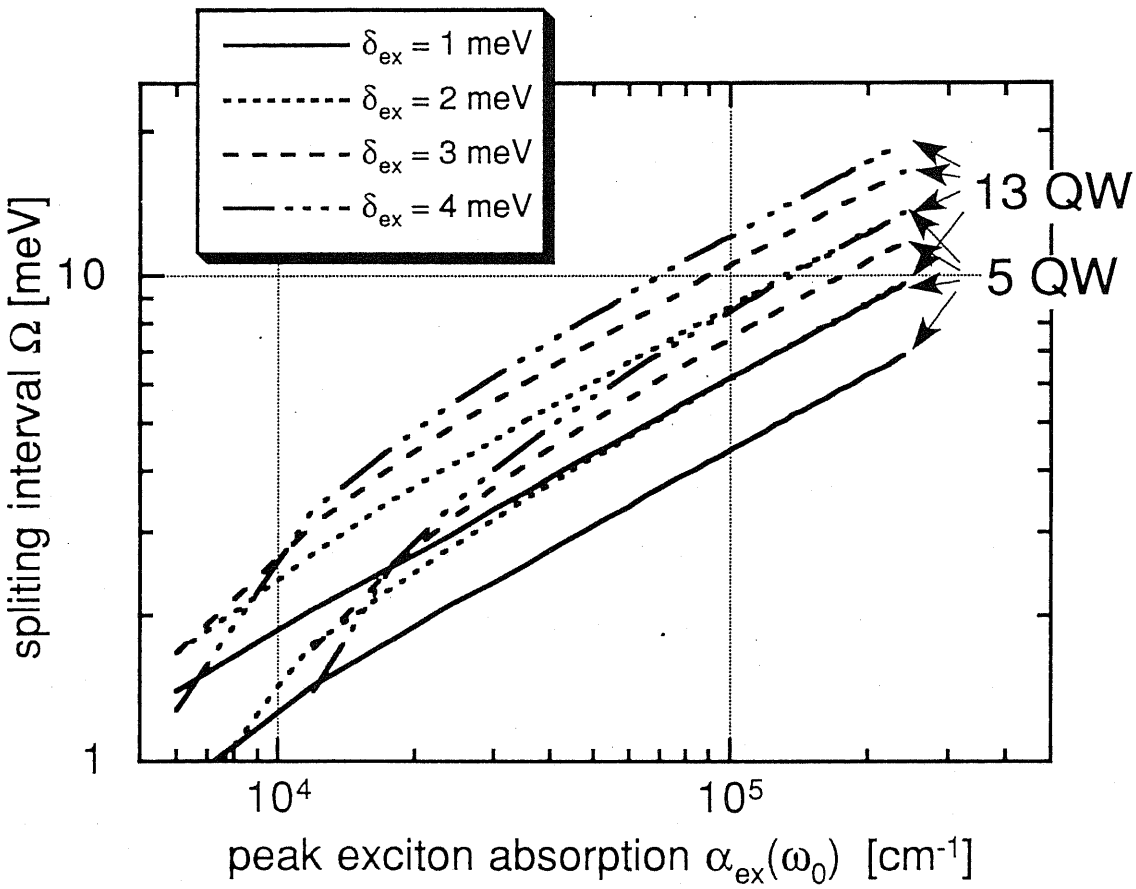

Figure 4.7: Calculated energy interval of exciton polariton mode splitting Ω as a function of peak exciton absorption $\alpha_{ex}(\omega_0)$ for the microcavity with 5 and 13 QWs. Solid, short-dashed, long-dashed, and solid-and-dashed lines show the data by full width at half maximum δ_{ex} is 1.0, 2.0, 3.0, and 4.0 meV, respectively.

Chapter 5

Conclusion

The author studied the magnetoexciton properties in quantum nanostructures and microcavities to clarify the phenomena of low dimensional carriers and photons in semiconductor.

In Chapter 2, the exciton properties were calculated by the theory assuming anisotropic 3D parabolic potential and Coulomb interaction within an electron–hole pair. For QWs, QWRs, QDs, and intermediate dimensional quantum nanostructures with and without magnetic field, the exciton properties such as binding energy, wavefunction, and exciton oscillator strength have been calculated. The magnetic field effect on those exciton properties was found to strongly depend on the confinement structures.

In Chapter 3, the dependence of magnetoexciton properties on the confinement structures of QWRs was theoretically discussed by the variational method and the three dimensional Schrödinger equation. The calculation was compared to the experiments of previous works for those anisotropy, the dependence on lateral confinement widths, and the dependence on structures and on angles of applied magnetic field.

The theory including Coulomb interaction and 2D anisotropic confinement shows

the importance of Coulomb interaction for the analysis. In addition, the theory including detailed structure configuration shows magnetoexciton properties are sensitive to the cross section of QWRs and the direction of applied magnetic fields. Moreover, the results show the experimental results of the magneto-PL are accurately described by the 1D magnetoexciton effect. These results clearly demonstrate that the magnetoexciton effect is important to analyze the magneto-optical properties in QWRs.

In Chapter 4, the measurement of the exciton-polariton mode splitting under a high magnetic field up to 14.5 T with different number of QWs embedded in microcavity was investigated. Moreover, the dependence of the strength of interaction between magnetoexciton and photon on the magnetic field was presented with the theoretical analysis.

In the measurement, continuous tuning-detuning of exciton and photon mode by applied magnetic field was realized for the first time. The enhancement of magnetoexciton–photon interaction has been found with increase of magnetic field. The theoretical analysis has clearly explained the experimental results of the samples with 5 QWs and also with 13 QWs, showing these properties are mainly caused by the increase of exciton oscillator strength due to the magnetic field. In addition, the large enhancement of the oscillator strength shows the possibility of the cavity electromagnetic field effect on the magnetoexciton.

The author hopes the present study contributes to accurate understanding of new phenomena in the electronic and optical confinement and its application to future novel devices.

Bibliography

[1] Y. Arakawa and H. Sakaki. Multidimensional quantum well laser and temperature dependence of its threshold current. *Appl. Phys. Lett. (USA)*, Vol. 40, No. 11, pp. 939–41, June 1982.

[2] M. Asada, Y. Miyamoto, and Y. Suematsu. Gain and the threshold of three dimensional quantum-box lasers. *IEEE J. Quantum Electron. (USA)*, Vol. QE-22, No. 9, pp. 1915–21, September 1986.

[3] Y. Arakawa, K. Vahala, and A. Yariv. Quantum noise and dynamics in quantum well and quantum wire lasers. *Appl. Phys. Lett. (USA)*, Vol. 45, No. 9, pp. 950–2, November 1984.

[4] Hiroyuki Sakaki. Scattering suppression and high-mobility effect of size-quantized electrons in ultrafine semiconductor wire structures. *Jpn. J. Appl. Phys. (Japan)*, Vol. 19, No. 12, pp. L735–8, December 1980.

[5] Y. Arakawa, Y. Nagamune, M. Nishioka, and S. Tsukamoto. Fabrication and optical properties of GaAs quantum wires and dots by MOCVD selective growth. *Semicond. Sci. Technol. (UK)*, Vol. 8, No. 6, pp. 1082–8, June 1993.

[6] E. Kapon. Quantum wire lasers grown by OMCVD on nonplanar substrates. *Optoelectron., Devices Technol. (Japan)*, Vol. 8, No. 4, pp. 429–60, December 1993.

[7] E. Yablonovitch. Inhibited spontaneous emission in solid-state physics and electronics. *Phys. Rev. Lett. (USA)*, Vol. 58, No. 20, pp. 2059–62, May 1987.

[8] Y. Arakawa and A. Yariv. Quantum well lasers-gain, spectra, dynamics. *IEEE J. Quantum Electron. (USA)*, Vol. QE-22, No. 9, pp. 1887–99, September 1986.

[9] Y. Nagamune, Y. Arakawa, S. Tsukamoto, M. Nishioka, S. Sasaki, and N. Miura. Photoluminescence spectra and anisotropic energy shift of GaAs quantum wires in high magnetic fields. *Phys. Rev. Lett. (USA)*, Vol. 69, No. 20, pp. 2963–6, November 1992.

[10] A.S. Plaut, K. Kash, E. Kapon, D.M. Hwang, and E. Colas. Magneto-optics of quantum wires grown on V-grooved substrates. *Surf. Sci. (Netherlands)*, Vol. 305, No. 1-3, pp. 576–9, March 1994.

[11] Y. Nagamune, T. Tanaka, T. Kono, S. Tsukamoto, M. Nishioka, Y. Arakawa, K. Uchida, and N. Miura. Observation of enhanced lateral confinement of excitons in GaAs quantum wires with various sizes (7-30 nm) by magnetophotoluminescence measurements. *Appl. Phys. Lett. (USA)*, Vol. 66, No. 19, pp. 2502–4, May 1995.

[12] T. Someya, H. Akiyama, and H. Sakaki. Laterally squeezed excitonic wave function in quantum wires. *Phys. Rev. Lett. (USA)*, Vol. 74, No. 18, pp. 3664–7, May 1995.

[13] Y. Nagamune, M. Nishioka, S. Tsukamoto, and Y. Arakawa. GaAs quantum dots with lateral dimension of 25 nm fabricated by selective metalorganic chemical vapor deposition growth. *Appl. Phys. Lett. (USA)*, Vol. 64, No. 19, pp. 2495–7, May 1994.

[14] K. Yanata and Y. Oka. Magneto-optical studies on $Cd_{1-x}Mn_xSe$ quantum dots. *Jpn. J. Appl. Phys. Suppl. (Japan)*, Vol. 34, No. SUPPL.34-1, pp. 164–6, 1994.

[15] R.E. Sherriff and R.P. Devaty. Size effects in the far-infrared magneto-optical absorption of small bismuth particles. *Phys. Rev. B, Condens. Matter (USA)*, Vol. 48, No. 3, pp. 1525–36, July 1993.

[16] K. Ando, Y. Yamada, and V.A. Shakin. Magneto-optical study of quantum confinement in Cd(S,Se) quantum dots. *Phys. Rev. B, Condens. Matter (USA)*, Vol. 47, No. 20, pp. 13462–5, May 1993.

[17] Kohki Mukai, Nobuyuki Ohtsuka, Mitsuru Sugawara, and Susumu Yamazaki. Self-formed $In_{0.5}Ga_{0.5}As$ quantum dots on GaAs substrates emitting at 1.3 μm. *Jpn. J. Appl. Phys. 2, Lett. (Japan)*, Vol. 33, No. 12A, pp. L1710–12, December 1994.

[18] H. Noguchi, H. Sakaki, T. Takamasu, and N. Miura. Observation of magnetophonon resonance in the miniband transport in semiconductor superlattices. *Phys. Rev. B, Condens. Matter (USA)*, Vol. 45, No. 20, pp. 12148–51, May 1992.

[19] K.-F. Berggren, T.J. Thornton, D.J. Newson, and M. Pepper. Magnetic depopulation of 1D subbands in a narrow 2D electron gas in a GaAs:AlGaAs

heterojunction. *Phys. Rev. Lett. (USA)*, Vol. 57, No. 14, pp. 1769–72, October 1986.

[20] S.K. Yip. Magneto-optical absorption by electrons in the presence of parabolic confinement potentials. *Phys. Rev. B, Condens. Matter (USA)*, Vol. 43, No. 2, pp. 1707–18, January 1991.

[21] V. Fock. Bemerkung zur Quantelung des harmonischen Oszillators im Magnetfeld. *Z. Phys.*, Vol. 47, pp. 446–8, 1928.

[22] C.T. Liu, K. Nakamura, D.C. Tsui, K. Ismail, D.A. Antoniadis, and Henry I. Smith. Magneto-optics of a quasi-zero-dimensional electron gas. *Appl. Phys. Lett. (USA)*, Vol. 55, No. 2, pp. 168–70, July 1989.

[23] A.V. Madhav and T. Chakraborty. Electronic properties of anisotropic quantum dots in a magnetic field. *Phys. Rev. B, Condens. Matter (USA)*, Vol. 49, No. 12, pp. 8163–8, March 1994.

[24] R. Haupt and L. Wendler. Electronic properties and electron-phonon interaction in an array of anisotropic parabolic quantum dots in the presence of a magnetic field. *Solid-State Electron. (UK)*, Vol. 37, No. 4-6, pp. 1153–7, April-June 1994.

[25] V. Halonen, Tapash Chakraborty, and P. Pietiläinen. Excitons in a parabolic quantum dot in magnetic fields. *Phys. Rev. B, Condens. Matter (USA)*, Vol. 45, No. 11, pp. 5980–5, March 1992.

[26] A.B. Dzyubenko and A.Yu. Sivachenko. Magnetoexcitons in zero-dimensional parabolic quantum dots. *J. Phys. IV, Colloq. (France)*, Vol. 3, No. C5, pp. 381–4, October 1993.

[27] S. Nomura, Y. Segawa, and T. Kobayashi. Confined excitons in a semiconductor quantum dot in a magnetic field. *Phys. Rev. B, Condens. Matter (USA)*, Vol. 49, No. 19, pp. 13571–82, May 1994.

[28] S. Nomura, X. Zhao, O. Schoenfeld, K. Misawa, T. Kobayashi, Y. Segawa, Y. Aoyagi, and T. Sugano. Magnetic field effects in direct- and indirect-gap semiconductor quantum dots. *Jpn. J. Appl. Phys. Suppl. (Japan)*, Vol. 34, No. SUPPL.34-1, pp. 125–7, 1994.

[29] S. Jaziri. Effects of electric and magnetic fields on excitons in quantum dots. *Solid State Commun. (USA)*, Vol. 91, No. 2, pp. 171–5, July 1994.

[30] H. Yokoyama. Physics and device applications of optical microcavities. *Science (USA)*, Vol. 256, No. 5053, pp. 66–70, April 1992.

[31] Y. Yamamoto and R.E. Slusher. Optical processes in microcavities. *Phys. Today (USA)*, Vol. 46, No. 6, pp. 66–73, June 1993.

[32] E.M. Purcell. Spontaneous emission probabilities at radio frequancies. *Phys. Rev. (USA)*, Vol. 69, p. 681, 1946.

[33] M. Yamanishi. Controlled spontaneous emission from semiconductor microcavities. *Phys. Status Solidi B (Germany)*, Vol. 188, No. 1, pp. 181–90, March 1995.

[34] Claude Weisbuch. Semiconductors quantum wells and microcavities. *Jpn. J. Appl. Phys. Suppl. (Japan)*, Vol. 34, No. SUPPL.34-1, pp. 247–50, 1994.

[35] T. Yamauchi, Y. Arakawa, and M. Nishioka. Enhanced and inhibited spontaneous emission in GaAs/AlGaAs vertical microcavity lasers with two kinds of quantum wells. *Appl. Phys. Lett. (USA)*, Vol. 58, No. 21, pp. 2339–41, May 1991.

[36] Y. Yamamoto, S. Machida, Y. Horikoshi, K. Igeta, and G. Bjork. Enhanced and inhibited spontaneous emission of free excitons in GaAs quantum wells in a microcavity. *Opt. Commun. (Netherlands)*, Vol. 80, No. 5-6, pp. 337–42, January 1991.

[37] K. Nishioka, K. Tanaka, I. Nakamura, Y. Lee, and M. Yamanishi. Observation of cavity effect on spontaneous emission lifetime in AlGaAs quantum microcavities using continuous tuning of emission wavelength. *Appl. Phys. Lett. (USA)*, Vol. 63, No. 21, pp. 2944–6, November 1993.

[38] T. Arakawa, M. Nishioka, Y. Nagamune, and Y. Arakawa. Fabrication of vertical-microcavity quantum wire lasers. *Appl. Phys. Lett. (USA)*, Vol. 64, No. 17, pp. 2200–2, April 1994.

[39] M. Nishioka, R. Schur, M. Kitamura, H. Watabe, and Y. Arakawa. Light emission from vertical-microcavity quantum dot laser structures. In *Program of Third International Symposium on "New Phenomena in Mesoscopic Structures ", Maui, Hawaii, USA*, pp. 457–9. Japan Society for Promotion of Science, December 1995.

[40] M. Nishioka, R. Schur, M. Kitamura, H. Watabe, and Y. Arakawa. Light emission from vertical-microcavity quantum dot laser structures. *Physica B (Netherlands)*, 1996. to be published.

[41] C. Weisbuch, M. Nishioka, A. Ishikawa, and Y. Arakawa. Observation of the coupled exciton-photon mode splitting in a semiconductor quantum microcavity. *Phys. Rev. Lett. (USA)*, Vol. 69, No. 23, pp. 3314–17, December 1992.

[42] T. B. Norris, J.-K. Rhee, C.-Y. Sung, Y. Arakawa, M. Nishioka, and C. Weisbuch. Time-resolved vacuum Rabi oscillations in a semiconductor quantum microcavity. *Phys. Rev. B, Condens. Matter (USA)*, Vol. 50, No. 19, pp. 14663–6, November 1994.

[43] J. Jacobson, S. Pau, H. Cao, G. Björk, and Y. Yamamoto. Observation of exciton-polariton oscillating emission in a single-quantum-well semiconductor microcavity. *Phys. Rev. A, Condens. Matter (USA)*, Vol. 51, No. 3, pp. 2542–44, March 1995.

[44] T. A. Fisher, A. M. Afshar, D. M. Whittaker, M. S. Skolnick, J. S. Roberts, G. Hill, and M. A. Pate. Electric-field and temperature tuning of exciton-photon coupling in quantum microcavity structures. *Phys. Rev. B, Condens. Matter (USA)*, Vol. 51, No. 4, pp. 2600–3, January 1995.

[45] R. Houdré, R.P. Stanley, U. Oesterle, M. Ilegems, and C. Weisbuch. Room temperature exciton-photon Rabi splitting in a semiconductor microcavity. *J. Phys. IV (France)*, Vol. 3, pp. 51–8, October 1993.

[46] R. Houdré, R.P. Stanley, U. Oesterle, M. Ilegems, and C. Weisbuch. Room-temperature cavity polaritons in a semiconductor microcavity. *Phys. Rev. B, Condens. Matter (USA)*, Vol. 49, No. 23, pp. 16761–4, June 1994.

[47] J. Tignon, P. Voisin, C. Delalande, M. Voos, R. Houdré, U. Oesterle, and R. P. Stanley. From Fermi's golden rule to the vacuum Rabi splitting: magnetopolaritons in a semiconductor optical microcavity. *Phys. Rev. Lett. (USA)*, Vol. 74, No. 20, pp. 3967–9, May 1995.

[48] R. Houdré, J. L. Gibernon, P. Pellandini, R. P. Stanley, U. Oesterle, C. Weisbuch, J. O'Gorman, B. Roycroft, and M. Ilegems. Saturation of the strong-coupling regime in a semiconductor microcavity: free-carrier bleaching of cavity polaritons. *Phys. Rev. B, Condens. Matter (USA)*, Vol. 52, No. 11, pp. 7810–13, September 1995.

[49] Z.L. Zhang, M. Nishioka, and Y. Arakawa. Dependence of photon-exciton interaction in microcavities on the number of quantum wells. In *Technical Digest of the Pacific Rim Conference on Lasers and Electro-Optics (CLEO), Chiba, Japan*, p. 92, July 1995.

[50] L.C. Andreani. Polaritons in multiple quantum wells. *Phys. Status Solidi B (Germany)*, Vol. 188, No. 1, pp. 29–42, March 1995.

[51] R. Houdré, C. Weisbuch, R.P. Stanley, U. Oesterle, P. Pellandini, and M. Ilegems. Measurement of cavity-polariton dispersion curve from angle-resolved photoluminescence experiments. *Phys. Rev. Lett. (USA)*, Vol. 73, No. 15, pp. 2043–6, October 1994.

[52] Z.L. Zhang, M. Nishioka, C. Weisbuch, and Y. Arakawa. Demonstration of confined optical field effect in a vertical microcavity by examining the low temperature photon-exciton interaction in two kinds of quantum wells. *Appl. Phys. Lett. (USA)*, Vol. 64, No. 9, pp. 1068–70, February 1994.

[53] D.S. Citrin. Controlled exciton spontaneous emission in optical-microcavity-embedded quantum wells. *IEEE J. Quantum Electron. (USA)*, Vol. 30, No. 4, pp. 997–1014, April 1994.

[54] H. Cao, J. Jacobson, G. Björk, S. Pau, and Y. Yamamoto. Observation of dressed-exciton oscillating emission over a wide wavelength range in a semiconductor microcavity. *Appl. Phys. Lett. (USA)*, Vol. 66, No. 9, pp. 1107–9, February 1995.

[55] S. Pau, G. Björk, J. Jacobson, H. Cao, and Y. Yamamoto. Stimulated emission of a microcavity dressed exciton and suppression of phonon scattering. *Phys. Rev. B, Condens. Matter (USA)*, Vol. 51, No. 11, pp. 7090–100, March 1995.

[56] E. Hanamura, J. Inoue, and F. Yura. Dressed excitons in microcavity. *J. Nonlinear Opt. Phys. Mater. (Singapore)*, Vol. 4, No. 1, pp. 13–25, January 1995.

[57] T. Tanaka, J. Singh, Y. Arakawa, and P. Bhattacharya. Near band edge polarization dependence as a probe of structural symmetry in GaAs/AlGaAs quantum dot structures. *Appl. Phys. Lett. (USA)*, Vol. 62, No. 7, pp. 756–8, February 1993.

[58] R. Tsu and L. Ioriatti. Longitudinal dielectric constant for quantum wells. *Superlattices & Microstruct. (UK)*, Vol. 1, No. 4, pp. 295–7, 1985.

[59] Masaki Shinada and Satoru Sugano. Interband optical transition in extremely anisotropic semiconductors. I. Bound and unbound exciton absorption. *J. Phys. Soc. Japan (Japan)*, Vol. 21, No. 10, pp. 1936–46, October 1966.

[60] Weiming Que. Excitons in quantum dots with parabolic confinement. *Phys. Rev. B, Condens. Matter (USA)*, Vol. 45, No. 19, pp. 11036–41, May 1992.

[61] Marcos H. Degani and Oscar Hipólito. Exciton binding energy in quantum-well wires. *Phys. Rev. B, Condens. Matter (USA)*, Vol. 35, No. 17, pp. 9345–8, June 1987.

[62] M. Sugawara, N. Okazaki, T. Fujii, and S. Yamazaki. Diamagnetic shift and oscillator strength of two-dimensional excitons under a magnetic field in $In_{0.53}Ga_{0.47}As/InP$ quantum wells. *Phys. Rev. B, Condens. Matter (USA)*, Vol. 48, No. 12, pp. 8848–56, September 1993.

[63] T. Yamauchi, Y. Arakawa, and J.N. Schulman. Tight-binding analysis of the conduction-band structure in quantum wires. *Appl. Phys. Lett. (USA)*, Vol. 57, No. 12, pp. 1224–6, September 1990.

[64] Y. Nagamune, T. Kono, S. Tsukamoto, M. Nishioka, and Y. Arakawa. Angle-resolved magneto-PL spectra in triangular-shaped GaAs quantum wires. In *Extended Abstracts (The 41st Spring Meeting, 1994); The Japan Society of Applied Physics and Related Societies*, No. 3, p. 1168, March 1994. in Japanese.

[65] E. Kapon, K. Kash, E.M. Clausen, Jr., D.M. Hwang, and E. Colas. Luminescence characteristics of quantum wires grown by organometallic chemical vapor deposition on nonplanar substrates. *Appl. Phys. Lett. (USA)*, Vol. 60, No. 4, pp. 477–9, January 1992.

[66] S. Tsukamoto, Y. Nagamune, M. Nishioka, and Y. Arakawa. Fabrication of GaAs quantum wires ($\approx$ 10 nm) by metalorganic chemical vapor selective deposition growth. *Appl. Phys. Lett. (USA)*, Vol. 63, No. 3, pp. 355–7, July 1993.

[67] M. Kohl, D. Heitmann, P. Grambow, and K. Ploog. One-dimensional magnetoexcitons in GaAs/$Al_xGa_{1-x}As$ quantum wires. *Phys. Rev. Lett. (USA)*, Vol. 63, No. 19, pp. 2124–7, November 1989.

[68] S. Tsukamoto, Y. Nagamune, M. Nishioka, and Y. Arakawa. Fabrication of GaAs arrowhead-shaped quantum wires by metalorganic chemical vapor deposition selective growth. *Appl. Phys. Lett. (USA)*, Vol. 62, No. 1, pp. 49–51, January 1993.

[69] S. Tarucha, H. Okamoto, Y. Iwasa, and N. Miura. Exciton binding energy in GaAs quantum wells deduced from magneto-optical absorption measurement. *Solid State Commun. (USA)*, Vol. 52, No. 9, pp. 815–9, 1984.

[70] Max Born and Emil Wolf. *Principles of Optics.* Pergamon, Oxford, 6 edition, 1986.

[71] Y. Zhu, D.J. Gauthier, S.E. Morin, Wu Qilin, H.J. Carmichael, and T.W. Mossberg. Vacuum rabi splitting as a feature of linear-dispersion theory: analysis

and experimental observations. *Phys. Rev. Lett. (USA)*, Vol. 64, No. 21, pp. 2499–502, May 1990.

[72] Ronald L. Greene and K.K. Bajaj. Binding energies of wannier excitons in GaAs-$Ga_{1-x}Al_xAs$ quantum well structures. *Solid State Commun. (USA)*, Vol. 45, No. 9, pp. 831–5, 1983.

[73] I. Aksenov, J. Kusano, Y. Aoyagi, T. Sugano, T. Yasuda, and Y. Segawa. Effect of a magnetic field on the excitonic luminescence line shape in a quantum well. *Phys. Rev. B, Condens. Matter (USA)*, Vol. 51, No. 7, pp. 4278–84, February 1995.

[74] J.C. Maan, G. Belle, A. Fasolino, M Altarelli, and K. Ploog. Magneto-optical determination of exciton binding energy in GaAs-$Ga_{1-x}Al_xAs$ quantum wells. *Phys. Rev. B, Condens. Matter (USA)*, Vol. 30, No. 4, pp. 2253–6, August 1984.

[75] J.C. Maan, A. Fasolino, G. Belle, M. Altarelli, and K. Ploog. Interband magnetooptical experiments in $Ga_{1-x}Al_xAs$-GaAs quantum wells. *Physica B & C (Netherlands)*, Vol. 127BC, No. 1-3, pp. 426–32, December 1984.

[76] N. Miura, Y. Iwasa, S. Tarucha, and H. Okamoto. Magneto-optics of two-dimensional excitons in GaAs-AlAs heterostructures in high magnetic fields. In *Proceedings of 17th International Conference on the Physics of Semiconductors*, pp. 359–362, 1984.

Publications

1 Journals

[1] M. Nishioka, S. Tsukamoto, Y. Nagamune, T. Tanaka, Y. Arakawa, "Fabrication of InGaAs strained quantum wires using selective MOCVD growth on SiO_2-patterned GaAs substrate". *J. Cryst. Growth*, **124**, 502-6, (1992).

[2] T. Tanaka, J. Singh, Y. Arakawa, and P. Bhattacharya, "Near band edge polarization dependence as a probe of structural symmetry in GaAs/AlGaAs quantum dot structures". *Appl. Phys. Lett.*, **62**, 756-8, (1993).

[3] T. Tanaka, T. Yamauchi, Y. Arakawa, and J. N. Schulman, "Cross sectional shape dependence of quantum wire band structures and optical matrix elements ". *Jpn. J. Appl. Phys.*, **32**, L1592-5, (1993).

[4] T. Tanaka and Y. Arakawa, "Analytical study of one dimensional electron gas confined by a harmonic potential in a magnetic field". **生産研究**, **46**, 41-44, (1994).

[5] M. Willatzen, T. Tanaka, Y. Arakawa, and J. Singh, "Polarization dependence of optoelectronic properties in quantum dots and quantum wires—— Consequences of valence-band mixing". *IEEE J. Quantum Electron.*, **QE30**, 640-53, (1994).

[6] T. Tanaka, Y. Arakawa, and G. W. E. Bauer, "Magnetoexcitons in quantum wires with an anisotropic parabolic potential". *Phys. Rev.*, **B50**, 7719-23, (1994).

[7] Y. Nagamune, T. Tanaka, T. Kono, S. Tsukamoto, M. Nishioka, Y. Arakawa, K. Uchida, and N. Miura, "Observation of enhanced lateral confinement of excitons in GaAs quantum wires with various sizes (7–30 nm) by magnetophotoluminescence measurements". *Appl. Phys. Lett.*, **66**, 2502-4, (1995).

2 International conferences

[1] T. Tanaka, J. Singh, Y. Arakawa, and P. Bhattacharya, "Theoretical study of polarization dependence of optical transition in quantum wires and dots using a formalism for 3-D confined structures". *19th International Symposium on Gallium Arsenide and Related Compounds*, September 1992, Karuizawa.

[2] T. Tanaka, Y. Nagamune, T. Kono, M. Nishioka, Y. Arakawa, K. Uchida, N. Miura, and G. E. W. Bauer, "Magneto-optical effect in GaAs quantum wires with various lateral width". *22nd International Conference on the Physics of Semiconductors*, August 1994, Vancouver.

3 Domestic conferences

[1] 田中琢爾, 山内忠昭, 荒川泰彦, "量子細線のバンド構造——断面形状依存性". 第 52 回応用物理学会学術講演会, 1991 年 9 月, 岡山.

[2] 西岡政雄、田中琢爾、塚本史郎、永宗靖、荒川泰彦 "MOCVD 選択成長による InGaAs 歪量子細線の作製". 第 39 回応用物理学関係連合講演会, 1992 年 3 月, 千葉.

[3] 荒川泰彦、塚本史郎、永宗靖、西岡政雄、石川明夫、田中琢爾, “MOCVD 選択成長による GaAs 量子細線の作製と光物性”. 第 39 回応用物理学関係連合講演会, 1992 年 3 月, 千葉.

[4] 田中琢爾, M. Willatzen, J. Singh, 荒川泰彦, “量子箱・量子細線の電子状態と光学特性——バンド混合効果と形状の揺らぎの影響”. 第 53 回応用物理学会学術講演会, 1992 年 9 月, 大阪.

[5] 田中琢爾, J. Singh, 荒川泰彦, “量子細線の電子状態の解析——界面揺らぎの影響”. 第 40 回応用物理学関係連合講演会, 1993 年 3 月, 東京.

[6] 田中琢爾, G. E. W. Bauer, 永宗靖, 荒川泰彦, “量子細線における励起子の磁場効果の解析”. 第 54 回応用物理学会学術講演会, 1993 年 9 月, 札幌.

[7] 河野隆司, 永宗靖, 田中琢爾, 西岡政雄, 内田和人, 三浦登, 荒川泰彦, “GaAs 量子細線の磁気 PL スペクトル: 細線幅依存性” 第 41 回応用物理学関係連合講演会, 1994 年 3 月, 東京.

[8] 田中琢爾, 永宗靖, 荒川泰彦, “量子細線の電子状態の解析——印加磁場角度依存性”. 第 55 回応用物理学会学術講演会, 1994 年 9 月, 名古屋.

[9] 田中琢爾, 荒川泰彦, “量子細線・量子ドットにおける励起子の振動子強度の磁場依存性”. 第 56 回応用物理学会学術講演会, 1995 年 8 月, 金沢.

[10] 田中琢爾, 荒川泰彦, “量子井戸を有する微小共振器構造における光子－磁気励起子結合効果”. 第 43 回応用物理学関係連合講演会, 1996 年 3 月, 埼玉. (講演予定)

Appendix A

Calculation Method to Integrate the Variational Function

The variational method mentioned in Eq. (2.1-2.26), Chapter 2 and in Eq. (4.1-4.3), Chapter 4 yields the integral

$$I_n = \int_0^\infty r^n \phi(r) dr, \tag{A.1}$$

where

$$\phi(r) = \exp(-\alpha r^2 - \beta r). \tag{A.2}$$

Following shows calculation method of the integral I_n.

Using the normal distribution function

$$f(x) = \frac{1}{\sqrt{2\pi}} \exp\left(-\frac{x^2}{2}\right), \tag{A.3}$$

and the error function

$$\mathrm{Erfc}(x) = \int_x^\infty f(t) dt, \tag{A.4}$$

the integral I_n is described by

$$I_n = \frac{J_n(a)}{\sqrt{(2\alpha)^{n+1}}} = \frac{a^{n+1} J_n(a)}{\beta^{n+1}}, \tag{A.5}$$

where

$$a = \beta/\sqrt{2\alpha}, \tag{A.6}$$

$a \geq 0$, and

$$J_n = \frac{1}{f(a)} \int_a^\infty (r-a)^n f(r) dr. \tag{A.7}$$

The differentials of Eq. (A.3), those linear combinations, and partial integral derive the integral J_n:

$$J_4(a) = (a^4 + 6a^2 + 3)\frac{\mathrm{Erfc}(a)}{f(a)} - (a^3 + 5a), \tag{A.8}$$

$$J_3(a) = (a^2 + 2) - (a^3 + 3a)\frac{\mathrm{Erfc}(a)}{f(a)}, \tag{A.9}$$

$$J_2(a) = (a^2 + 1)\frac{\mathrm{Erfc}(a)}{f(a)} - a, \tag{A.10}$$

$$J_1(a) = 1 - a\frac{\mathrm{Erfc}(a)}{f(a)}, \tag{A.11}$$

$$J_0(a) = \frac{\mathrm{Erfc}(a)}{f(a)}. \tag{A.12}$$

The integral I_n is calculated by Eqs. (A.5), (A.6), (A.8)–(A.12). They are numerically calculable with Fortran standard functions for $0 < a \lesssim 10$. However, in the range of $a \gtrsim 10$, the calculation by computer may include an error because of $f(a) \to 0$. The calculation is enabled using the expansion

$$\mathrm{Erfc}(x) = \frac{1}{2} - \frac{1}{\sqrt{2\pi}} \sum_{n=0}^{\infty} \frac{(-)^n x^{2n+1}}{n! 2^n (2n+1)}, \ (0 \leq x < 1) \tag{A.13}$$

$$\begin{aligned} \mathrm{Erfc}(x) &= \frac{f(x)}{x} \sum_{n=0}^{k} (-)^n \frac{(2n-1)!!}{x^{2n}} \\ &\quad + (-)^{(k+1)} \int_x^\infty \frac{(2k+1)!!}{t^{2(k+1)}} f(t) dt, \ (x > 1) \end{aligned} \tag{A.14}$$

At the limit of $a \to \infty$, the term $a^{n+1}J_n(a)$ in the Eq. (A.5) asymptotically reaches the following value

$$\lim_{a\to\infty} a^{n+1}J_n(a) = \lim_{\alpha\to+0,\beta\to1}\int_0^\infty x^n\phi(x)dx = n!. \tag{A.15}$$

At the other limit of $a \to +0$, the term $J_n(a)$ in the Eq. (A.5) asymptotically reaches the following value

$$\begin{aligned}\lim_{a\to+0} J_n(a) &= \lim_{\alpha\to+0,\alpha\to1/2}\int_0^\infty x^n\phi(x)dx \\ &= \begin{cases}(n-1)!!\sqrt{\dfrac{\pi}{2}} & (n \in \text{even}), \\ 2^{\frac{n-1}{2}}\left(\dfrac{n-1}{2}\right)! & (n \in \text{odd}).\end{cases}\end{aligned} \tag{A.16}$$

The parameter a determined by Eq. (A.6) is equivalent to the parameters t_ζ mentioned in Chapter 2, which describes the character of the variational function along the ζ axis, which can be more Gaussian-like or more Hydrogen-like.